Review in Advance first posted online on May , 2014. (Changes may still occur before final publication online and in print.)

Mechanistic Studies in Friction and Wear of Bulk Materials

W. Gregory Sawyer,[1] Nicolas Argibay,[2] David L. Burris,[3] and Brandon A. Krick[4]

[1]Department of Mechanical and Aerospace Engineering, University of Florida, Gainesville, Florida 32611; email: wgsawyer@ufl.edu

[2]Sandia National Laboratories, Albuquerque, New Mexico 87123

[3]Department of Mechanical Engineering, University of Delaware, Newark, Delaware 19716

[4]Department of Mechanical Engineering and Mechanics, Lehigh University, Bethlehem, Pennsylvania 18015

Annu. Rev. Mater. Res. 2014. 44:16.1–16.33

The *Annual Review of Materials Research* is online at matsci.annualreviews.org

This article's doi:
10.1146/annurev-matsci-070813-113533

Keywords

wear, friction, tribology, metals, PTFE, ionic solids, nanocomposites, electrical contacts

Abstract

From the context of a conte understanding of the phenomenological origins of friction and wear of materials, we review insightful contributions from recent experimental investigations of three classes of materials that exhibit uniquely contrasting tribological behaviors: metals, polymers, and ionic solids. We focus on the past decade of research by the community to better understand the correlations between environment parameters, materials properties, and tribological behavior in systems of increasingly greater complexity utilizing novel synthesis and in situ experimental techniques. In addition to such review, and a half-century after seminal publications on the subject, we present recently acquired evidence linking anisotropy in friction response with anisotropy in wear behavior of crystalline ionic solids as a function of crystallographic orientation. Although the tribological behaviors of metals, polymers, and ionic solids differ widely, it is increasingly more evident that the mechanistic origins (such as fatigue, corrosion, abrasion, and adhesion) are essentially the same. However, we hope to present a clear and compelling argument favoring the prominent and irreplaceable role of in situ experimental techniques as a bridge between fundamental atomistic and molecular processes and emergent behaviors governing tribological contacts.

1. INTRODUCTION

Encounters with friction and wear occur on a daily basis, and there exist many situations in which friction and wear severely limit the performance of moving mechanical assemblies or altogether prohibit motion over prolonged operation. Integrated approaches using high-resolution scientific instrumentation and model materials as samples are providing a means to develop a deeper understanding of the underlying mechanisms in friction and wear of materials (**Figure 1**).

Materials tribology, which is the study of friction and wear of materials, is an intrinsically multiscale and multidisciplinary endeavor. As illustrated in **Figure 2**, the combined access to detailed, large-scale molecular simulations; exquisite control over interfacial composition and structure; and atomically specific tribological probes provide an opportunity to study the fundamental mechanisms of friction and wear, and such studies are capable of widely impacting society and future technologies.

Analytical models, like those from Tomlinson (1) and Frenkel & Kontorova (2), have given the theoretical context for molecular friction and wear, whereas single-asperity experiments with scanning probe methods have qualitatively supported the models. Mate et al. (3), for example, first observed atomic stick slip. Other investigators have shown qualitative agreement between experiment and theoretical predictions of frictional anisotropy and superlubricity (4–6), temperature effects (7–10), and speed effects (11, 12). Although encouraging agreement has been observed between

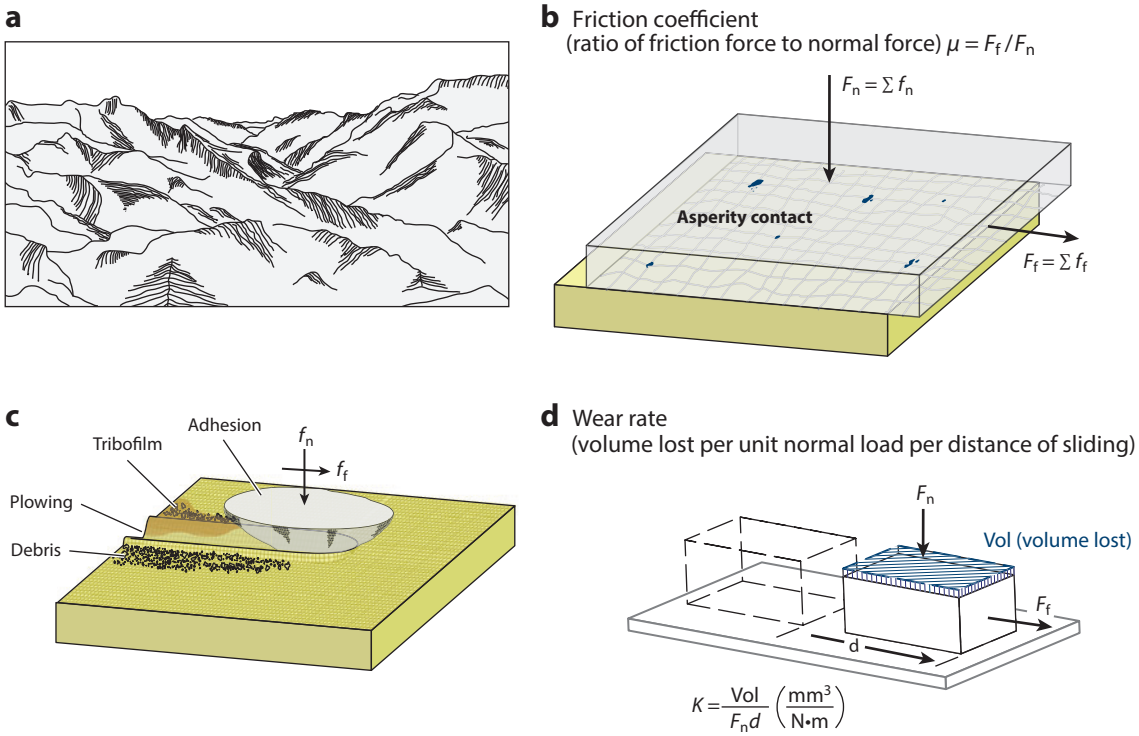

Figure 1

(*a*) All surfaces are rough, and this roughness extends to all length scales from the atomic scale to the macroscale. (*b*) The peaks (protuberances or asperities) are the high points of surfaces and are involved in multiple microscopic contacts that are distributed across the contacting surfaces. (*c*) These asperity contacts are typically nanoscopic and highly stressed. (*d*) An ensemble of these nanoscopic contacts collectively manifests the macroscopic parameters known as friction coefficient and wear rate.

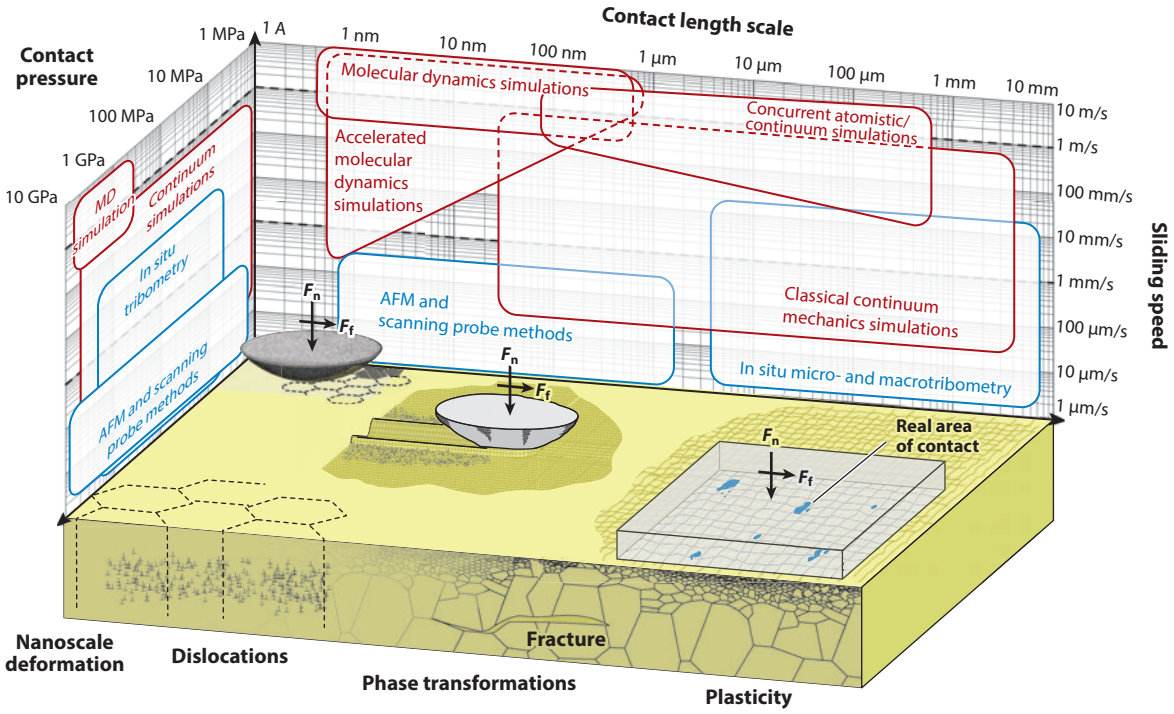

Figure 2

Materials tribology spans multiple length scales and timescales. There are currently areas of strong overlap between experimental capabilities and both numerical and theoretical modeling of tribological processes. AFM denotes atomic force microscopy.

theory and experiment, large gaps persist in our understanding of experimentally observed phenomena.

Advances in computational methods development and the corresponding large increases in computer resources over the past two decades have enabled atomic-scale simulations to have a profound impact on a variety of disciplines, including the areas of friction and wear (13–15). For example, there have been several simulation studies of nanoindentation (16–22), cutting (23–27), and scratching (28–31) of metal surfaces by nanometer-scale tips. These simulations have provided valuable insights into the mechanical responses of the surfaces, including hardness, dislocation generation, and elastic-to-plastic transition at the nanoscale. Additional simulations have investigated molecules and thin films trapped between sliding surfaces, including tribochemical reactions (32), the way in which long-chain hydrocarbons influence asperity interactions in sliding metal surfaces (20), and the role of adsorbed thin films on friction (33–36). The goal of the mitigation of wear through molecular-scale lubrication has been the emphasis of many simulations (37).

In the context of polymer tribology and in particular the tribology of polytetrafluoroethylene (PTFE) films, molecular dynamics (MD) simulations have been used to investigate atomic-scale friction at interfaces of self-mated PTFE constructs (38). The simulations demonstrated unequivocally that molecular structural orientation at the sliding interface strongly influences friction and wear, as indicated in **Figure 3**. Sliding of chains oriented parallel to the chain backbones resulted in low friction forces and in low barriers to interfacial slip and molecular reorganization at the surface. In contrast, sliding of chains oriented perpendicular to the chain backbones resulted in high friction forces and wear in the form of molecular reorientation and

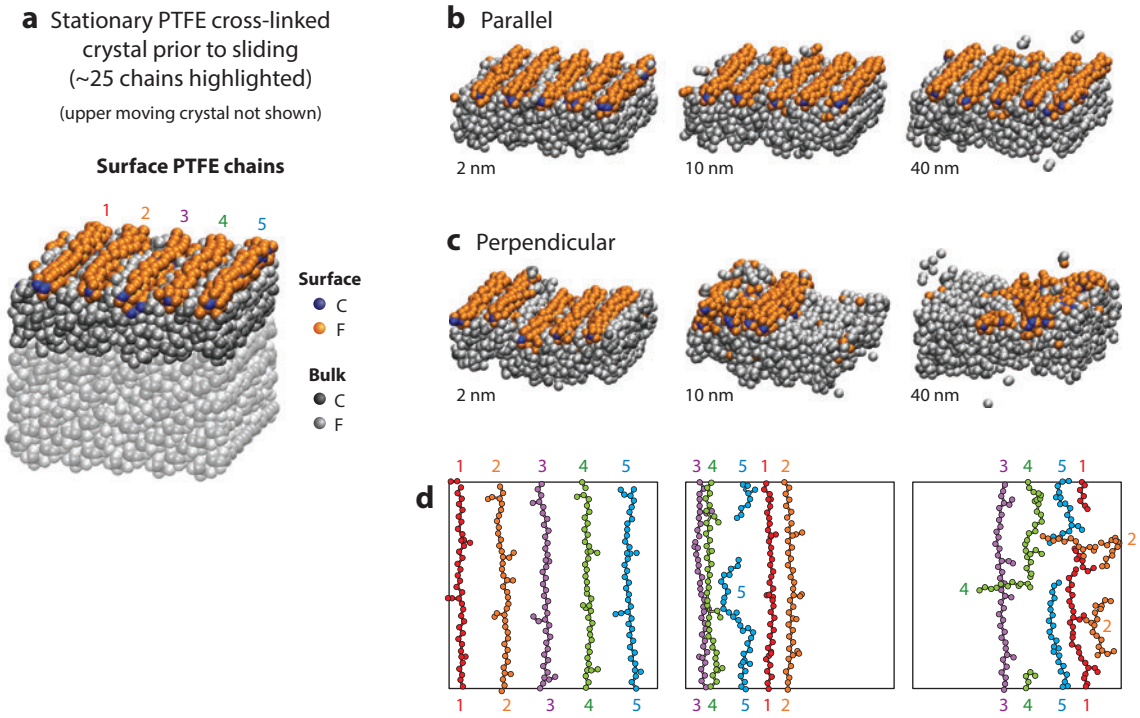

Figure 3

Snapshots from molecular dynamics simulations using many-body potentials of the evolution of oriented chains of polytetrafluoroethylene (PTFE) during sliding. The initial structure of the bottom surface is shown in panel *a*. The sequence in panel *b* illustrates the evolution of the bottom surface during sliding when the chains on the top (not shown) and bottom surfaces are oriented parallel to one another. In contrast, the sequence in panel *c* illustrates the evolution of the bottom surface when the chains on the top (not shown) and bottom surfaces are oriented perpendicular to one another. In the latter case, the simulations predict molecular-scale wear of the PTFE surface. In particular, the chains on the bottom surface deform, break, and are in the process of reorienting to line up with the direction of sliding, as indicated by the schematics of the numbered chains in panel *d*.

chain scission. These predictions were examined and validated by complementary experiments on oriented transfer films of PTFE (38). Microtribological measurements on these aligned films demonstrated a strong anisotropy in friction and wear, consistent with the MD simulation predictions. Specifically, the parallel sliding of oriented films produced low friction and wear, whereas perpendicular sliding led to higher friction, consistent with molecular reorientation.

Despite the important insights obtained from these types of simulations, several important limitations hinder their widespread utility. First, the computational system sizes are substantially smaller than the experimental systems by several orders of magnitude. This limits the size scales on which phenomena can occur in the simulations, potentially causing them to miss events that occur over a large scale. Second, dissipation timescales are much quicker computationally than in the experiments, which may also influence the mechanisms by which the surface responds to the applied forces. The short timescales of classical MD simulations are typically on the order of several nanoseconds and thus necessitate sliding rates that are frequently orders of magnitude faster than experimental rates. Third, due to the size and rates of MD simulations, the artificial addition of high cross-links or other tricks are often used to mimic entanglement. Finally, the contact pressures are frequently much higher in simulations than in experiments (for stability reasons

and to minimize the effects of thermal noise on the force measurements). As we move forward, timescales and simulation sizes must increase in an effort to meet single-asperity nanotribological experiments.

In this article, we review activities, primarily experimental, aimed at elucidating the various mechanisms that are involved in wear processes of metals, polymers, and ceramics. Far from an exhaustive study, we focus on the materials for which we have the most experience in the following categories: Cu, PTFE, and single-crystal ionic solids.

2. METALS AS A TRIBOLOGICAL MATERIAL

The development and widespread adoption of low-friction, highly durable, and superhard, solid-lubricant thin-film materials, such as hard-carbon (diamond-like carbon, diamond-like nanocomposites, and carbonitrides) and nanostructured or patterned coatings, have led to significant improvements in the reliability and efficiency of metal contacts in engineering applications ranging from automobile pistons and cylinders to cutting tools and ball bearings (39–42). Layered and composite thin films have provided an effective and economical means of tailoring the mechanical and chemical surface properties of relatively inexpensive and practical-to-manufacture bulk metal and alloy engineering materials. Fundamentally, thin films are implemented to mitigate the high wear and friction associated with the gross adhesion and plasticity exhibited by unlubricated and boundary-lubricated metal contacts. Electrical contacts are arguably the only remaining class of tribological contacts for which metal-on-metal friction and wear remain a topic of practical interest. In this application, the use of minimally insulating thin films, including passivating oxides, may cause prohibitive electrical losses.

2.1. Introduction to Friction and Wear Processes in Metal Contacts

The friction and wear of metals are a well-trodden area of research, with seminal contributions from Holm (43), Cocks (44), Greenwood (45), Tabor (46), and Antler (47, 48); Blau (49) has a nice review of this work. We summarize select research efforts from our laboratories and others that focus on the physics and chemistry of debris generation in sliding metal contacts. Recent experimental and theoretical efforts have focused on the development of materials solutions exhibiting higher efficiency and longevity in power and signal transfer applications such as rapidly switching microelectromechanical systems (MEMS) (50–53) and high-current-density electrical sliding contacts for power generation (54–67). In such applications, traditional approaches to engineering design—and even descriptions of wear processes, such as the wear mechanism maps developed by Lim (68) and Lim & Ashby (69) for steels—have limited applicability. Such pioneering efforts to unify wear behaviors over a wide range of contact pressures and sliding speeds do not account for complex environmental and system dependencies. The wear maps for steel (69) outlined the various mechanisms of wear for a self-mated steel on steel sliding contact. These mechanisms were delineated primarily along mechanistic lines associated with the temperature of the sliding contact.

A successful design approach for a notionally unlubricated sliding metal-on-metal contact requires the combined consideration of the mechanical properties, surface reactivity, deformation history, wear, and environmental dependencies of the contact materials. Such design strategies aim to synergistically yield beneficial surface reactions and consider competing mechanisms such as wear and solid diffusion–dominated processes. Examples of such behavior are grain boundary–dominated plasticity of nanocrystalline materials (70–72) and thermally and electrochemically activated degradation pathways of metal electrical contacts (73–75).

2.2. In Situ Triboelectrochemistry

The practice of mating metal with metal to transfer electrical current from stationary to moving components for signal transfer and power generation is likely to be at the forefront of materials challenges in an increasingly electrified world. Demands for higher reliability and efficiency and the rapidly growing use of dc motors and generators in the automotive and power generation industries (e.g., multimegawatt wind turbines) will lead to an increased demand for low-wear, low-electrical-loss, high-current-density electrical contacts. Perhaps one of the more exciting prospects in this field of research is that a more sophisticated understanding of the complex surface kinetics governing the friction, wear, and electrical contact resistance behavior of metal electrical sliding contacts will finally enable practical commercialization of the first and only motor/generator topologies to remain technologically impractical: the homopolar motor (Faraday 1821) and the homopolar generator (Faraday, 1831). Such motivations led to investigations in the 1980s on the wear behavior of metal sliding contacts for high-current-density applications in electric motors and generators. These investigations resulted in two important discoveries:

1. Reichner (64, 76) demonstrated that the use of humidified CO_2 environments was conducive to low wear [8×10^{-7} mm^3/(N·m)], friction ($\mu \sim 0.3$), and electrical contact resistance ($\sim$0.5 mΩ) of Cu electrical sliding contacts at current densities greater than 20 MA/m^2 and sliding speeds greater than 10 m/s.
2. Boyer and colleagues (60, 62, 77) found a current density threshold above which metal fiber brush wear rates bifurcated significantly depending on the polarity of the dc contact; the brush was either the positive element or the negative element in the electrical contact. The authors (60) had the brilliant insight that, with a sufficiently large enough voltage drop across the contact, the imposed potentials approached the natural oxidation potentials (78, 79).

In more recent investigations, a combination of macroscale multifiber brush (54–56, 80) and single-asperity in situ triboelectrochemistry experiments against Cu in ionic liquid solutions exhibiting surface chemistry products similar to those of humidified CO_2 (81) revealed that this environment produces reaction kinetics favoring the formation of thin copper carbonate and hydroxide species at rates similar to the rate of materials attrition (wear), providing thin, lubricous films of easily displaced material. X-ray diffraction (XRD) spectroscopy and electron microscopy revealed a prevailing lamellar wear particle morphology suggesting delamination wear (82–84), which is a surface fatigue wear process, of the Cu surfaces. The use of a higher-fatigue-strength Cu-Be alloy further reduced the wear rate by an order of magnitude so that it was above even the asymmetrical wear current density threshold. Researchers then postulated a more complete description of the mechanism for the asymmetrical wear behavior (54, 85). This description was founded on a concept originating in a relatively obscure 1926 publication by Roscoe (86), later described and elaborated upon by Buckley and others (87–89) in the 1950s and 1970s and referred to as the Roscoe effect.

The so-called Roscoe effect qualitatively describes how the presence of hard-surface film increases the wear rate (**Figure 4**). Passivating oxide layers can produce a change in the prevailing mechanism of near-surface friction–induced plastic strain accommodation in a metal contact under conditions of moderate contact pressures. These layers can inhibit friction-induced dislocations from reaching the surface and relaxing (dislocation trapping). In high-current-density contacts, thick, electrochemically enhanced films more effectively trap dislocations and thereby accelerate delamination wear. Several groups have reported an analogous reduction in fatigue strength of thin metal films in fully reversed cyclic bending with and without passivating films (88–90). This reduction was demonstrated, perhaps most clearly via transmission electron microscopy by Nicola

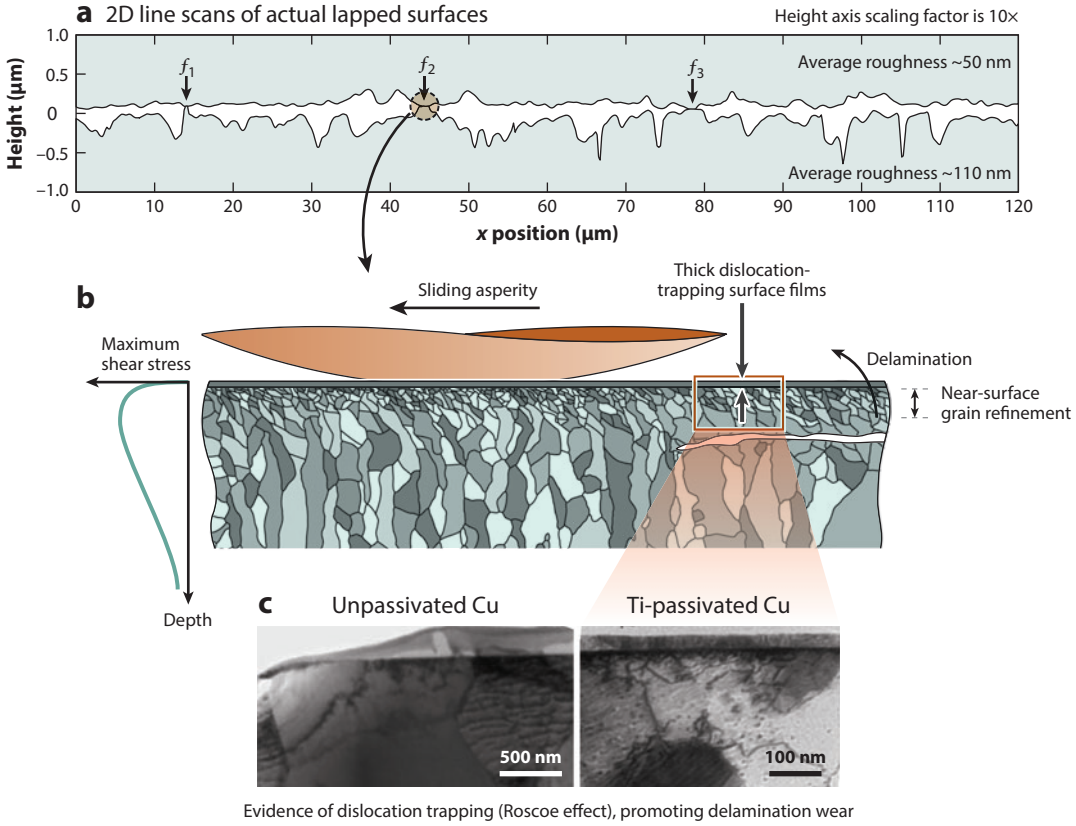

Figure 4

(*a*) Cross-sectional view of a real contact between polished metal surfaces. (*b*) Diagram of delamination wear in a mildly wearing, otherwise unlubricated metal contact. (*c*) Cross-sectional transmission electron microscopy images (from Reference 91) of fatigued (fully reversed, bulge test) Cu films both unpassivated (*left*) and Ti passivated (*right*), demonstrating the trapping of dislocations that enhances near-surface damage accumulation rates and delamination wear [the Roscoe effect (86, 87)].

et al. (91), to be a function of enhanced strain energy accumulation due to near-surface dislocation trapping.

Enhanced or inhibited surface reaction kinetics leading to the formation of passivating and lubricous films affects the rate of surface fatigue damage. This phenomenon causes a bifurcation in wear rate when electrochemical potential across a metal sliding electrical contact approaches the natural oxidation potential. This sophisticated understanding of the prevailing wear mechanisms in high-current-density Cu electrical sliding contacts (**Figure 5**), summarized in References 54 and 85, provides the motivation for triboelectrochemistry investigations with metallic contacts in aqueous ionic solutions that (*a*) exhibit favorable surface reaction kinetics for the formation of soft, lubricous, and perhaps even electrically conductive thin films and (*b*) enhance the wear performance of Cu electrical contacts.

In situ triboelectrochemistry remains a relatively unexplored research arena with significant potential for innovation. In a 2008 review, Mischler (92) evaluated the state of experimental techniques and analysis of triboelectrochemical data and provided a survey of the latest research efforts and materials systems investigated. The use of potential/pH equilibrium (Pourbaix) diagrams (93)

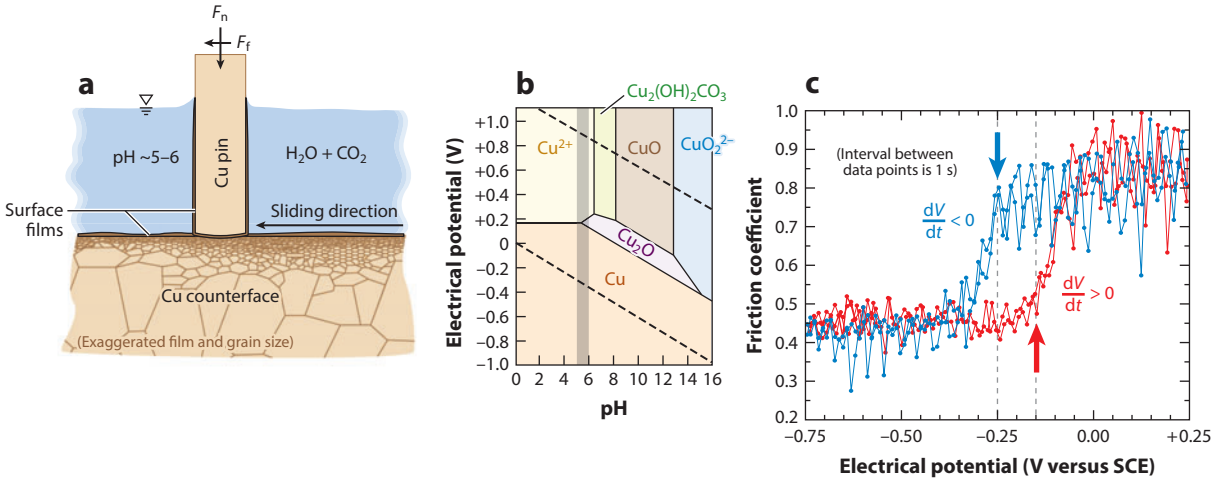

Figure 5

(*a*) A sliding contact of a self-mated Cu-on-Cu contact in a slightly acidic aqueous environment. (*b*) Equilibrium (Pourbaix) diagram for Cu-CO_2-H_2O (at 25°C). The diagram outlines the thermodynamic stability of the surface oxides. (*c*) Frictional voltammetry is a method that uses electrochemical techniques from corrosion experiments to dynamically and systematically vary the surface oxides during a friction experiment. The blue arrow shows the onset of electroreduction of CuO, $Cu(OH)_2$, and $CuCO_3$ at approximately −0.25 V versus SCE. The red arrow shows the onset of electroformation of CuO, $Cu(OH)_2$, and $CuCO_3$ at approximately −0.15 V versus SCE. SCE denotes saturated calomel electrode. Panel *c* adapted from Reference 81.

can be a useful road map. However, as Celis et al. (94) demonstrated for a Stellite and AISI 321 tribopair in an aqueous 0.5 M H_2SO_4 solution, the development of more-sophisticated analytical techniques and models is necessary to understand the arguably critical behavioral transitions that occur during tribocorrosion of metal contacts, when competing processes such as wear and surface reaction kinetics are not effectively described by equilibrium diagrams.

2.3. Low Wear with Unlubricated Metal Contacts

All metal-on-metal contacts experience wear. In engineering applications, the consequences of wear, wear debris, friction, and the changes in the surface topography and geometry define success or failure. Nanostructured metals have shown potential to produce low-wear metal-on-metal contacts. Progress in the area of physical vapor deposition (PVD) techniques such as pulsed laser deposition and e-beam deposition has enabled the ability to practically and economically synthesize nanostructured and nanocomposite thin-film materials exhibiting novel mechanical properties superior to the properties of traditional electroplated, sintered, or cast composites. For example, the practice of improving the wear resistance of Au coatings by electrodeposition of small amounts (0.1–1.0 wt%) of Ni or Co species in a primarily Au matrix, referred to as hard Au, has been used. Lo et al. (95) demonstrated that the increase in hardness and associated several-order-of-magnitude improvement in wear resistance are attributed primarily to Hall-Petch strengthening, and not to solution hardening, precipitation hardening, or strain hardening. In the study of the behavior of contact between nanostructured materials—those with features including grain sizes below 100 nm and molecularly thin layers of organic and inorganic lubricant films—the tribology community is rapidly approaching meaningful overlap between experiments and atomistic simulations. Although the predictive capabilities of simulations remain limited by computing power to length and temporal scales on the order of nanoseconds and micrometers, there have been

notable contributions by the modeling community to the collective fundamental understanding of the behavior of metal-on-metal contacts in a wide variety of operating conditions. For example, Yanson et al. (96) found a limiting electrical conductivity during the formation of monoatomic Au chains or nanowires in breaking Au-Au electrical contacts, with direct implications for the performance of MEMS. Similarly meaningful to the MEMS community, Gosvami et al. (97) investigated the temperature-dependent aging behavior (wear) of atomic-scale Au contacts. Utilizing massively parallel MD simulations to study strain hardening of polycrystalline Al, Yamakov et al. (98) verified a hypothesis based on experimental evidence that twin boundaries may cause dislocation pileups and enhance strain hardening. Other groups have investigated the relationship between mechanical strain and thermal energy on grain boundary mobility (99–102), relevant to understanding the stability of and propensity for relatively hard, wear-resistant nanocrystalline metals to undergo rapid grain growth. The rapid transition from grain boundary–dominated plasticity, characteristic of nanocrystalline materials, to traditional defect-dominated plasticity for coarser-grained (>100-nm) materials is currently the focus of much research interest and effort, the implications of which are discussed ahead. In the context of stick-slip behavior at a Pt/Au interface, Li et al. (103) effectively correlated experimental (atomic force microscopy) and MD simulations of stick-slip behavior, which is perhaps a step toward the holy grail of computational modeling, achieving predictive capability at the macroscopic scale. Atomistic simulations have the potential to provide unique fundamental insight into the complex interrelationship between the numerous, complex, and often stochastic and competing processes governing macroscale tribological behavior by allowing one to systematically deconstruct and artificially probe them independently.

After nearly a century of widespread use, hard Au, effectively Au wherein the grain size is controlled by the addition of grain boundary–segregated species (104) that pin boundaries, remains a mainstay in the design of robust electrical sliding contacts and an eminently relevant and uniquely practical material for the study of nanoscale phenomena of metal-on-metal contacts, both experimentally and computationally. Fundamentally, the increased strength and wear resistance are achieved by the dispersion of a relatively insoluble grain boundary–segregated, secondary metallic phase in a polycrystalline Au matrix that prevents recrystallization and grain boundary motion (which stabilizes grain boundaries) via Zener pinning. Average grain sizes on the order of 10–100 nm and 2–3-GPa hardness can be achieved on greater than 99-vol% pure Au by the addition of a grain boundary–stabilizing secondary species. PVD techniques were recently used to synthesize ceramic dispersion–strengthened Au films with tribological characteristics equivalent to those of traditional metal-hardened Au (105). This class of materials, ceramic dispersion–strengthened metal-matrix coatings, additionally helps mitigate a long-standing failure mode of traditional hard Au coatings: degradation in electrical contact resistance attributed to the formation of electrically insulating metal oxide films from the solid diffusion of non-noble-metal underlayer and codeposited species to the sliding surface (73, 74, 106–111).

In their 1979 paper, Rigney & Hirth (112) were perhaps the first to recognize that relatively low steady-state friction and wear behavior exhibited by some nominally unlubricated metal contacts may be attributed to the formation of a fine-grained, highly strained surface layer. However, as they point out, "...friction and wear are related, but not in a simple way, and accurate theoretical correlations of friction and wear have yet to be obtained." There has been emerging evidence of a correlation between (*a*) the transition to low-friction behavior (from $\mu > 1.0$ to $\mu \sim 0.2$) of mild-wearing, unlubricated metal contacts and (*b*) the formation of a nanograined surface layer of highly deformed base metal. Cross-sectional electron microscopy of surfaces of varying composition, initial grain size, and operating environment worn in to the low-friction regime have consistently revealed the presence of a thin, nanocrystalline surface layer not observed at elevated contact pressures and sliding speeds, which are correlated with more severe wear (113–115). The

transition to low-friction behavior of unlubricated, coarse-grained metal surfaces depends on contact pressure and sliding speed (113). In sufficiently aggressive contact conditions, gross wear outpaces the grain refinement process of near-surface material, which is needed to facilitate low friction ($\mu \sim 0.2$), although the stability and formation process of the nanocrystalline surface layer remains poorly understood (113). A 2010 review on the fatigue of nanocrystalline metals by Padilla & Boyce (116) provides some insight into the mechanics of crack initiation and propagation in nanocrystalline metals, although it is unclear how strain rate effects (speed dependencies) play a role in the formation process of a nanocrystalline layer during sliding. In situ deposition of thin solid-lubricant films, such as vapor-phase lubrication (55, 117, 118), was used to demonstrate that friction processes drive the surface recrystallization and grain refinement in metal-on-metal sliding contacts. When the lubricant films are sufficiently thin and lubricous, the wear of the metal surfaces abates, as long as the rate of deposition of the surface film outpaces the removal of the film.

The wear of sliding metal contacts of engineering alloys occurs through friction-induced surface deformation and reduced grain size at the interface. This process can be accelerated through the formation of thin, dense, and mechanically strong surface oxides that trap the friction-initiated dislocations and accumulate them beneath the contacting surface. As the process of frictional sliding repeats, this nanocrystalline zone increases in depth as the grain size at the surface continues to reduce. Correspondingly, the hardness of these surface layers increases at the cost of fatigue strength, which decreases. Eventually, this deformed and cold-worked nanocrystalline layer becomes so hard and brittle that it shatters off into fine wear particles or sheets that are ejected from the sliding contact (**Figure 6**). Recent work on the stability of nanocrystalline metals may present novel routes to understanding and engineering more-wear-resistant metal contacts. In a 2012 publication, Chookajorn et al. (119) demonstrated localized, intrinsic thermodynamic stability for a wide range of nanocrystalline binary metal alloys, in one example completely inhibiting the recrystallization of a W-Ti powder specimen of 20-nm average grain size. Specimens were prepared by ball milling and were exposed to 1,100°C for a 1-week period without a measurable

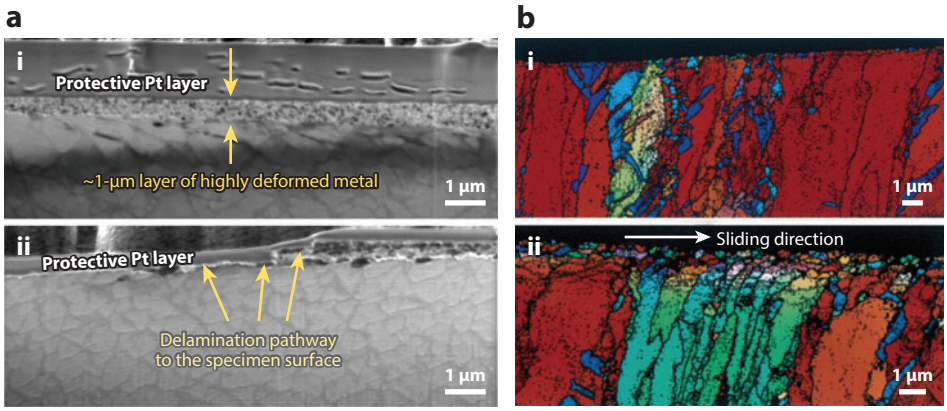

Figure 6

(*a*) Cross-sectional scanning electron microscopy images inside the wear track of a single-crystal Ni superalloy (CMSX-4) worn in against Si_3N_4 in N_2 (*i*) before and (*ii*) after a delamination wear event of the tribologically formed nanocrystalline surface layer. (*b*) An electron backscatter diffraction crystallographic orientation map adapted from Prasad et al. (115) showing cross-sectional views of (*i*) an unworn area and (*ii*) a worn-in area of a polycrystalline Ni substrate.

change in grain size. Two primary technical challenges limit the adoption of these thermally stable nanocrystalline metal alloys as practical engineering materials: (*a*) a demonstration of intrinsic or even partial stability under mechanical strain and (*b*) the development of thin-film or bulk synthesis and fabrication routes.

The present cross section of recent advances in the understanding of the processes governing the wear and friction of metals demonstrates that, even though this is perhaps the oldest and most intensely investigated class of tribological materials, there is plenty of room at the interface for influential and fundamental discovery.

3. POLYMERS AS A TRIBOLOGICAL MATERIAL

3.1. Introduction to Polymers in Tribology

Whereas metallic and ceramic surfaces are rarely used in notionally unlubricated applications, polymers not only are used in unlubricated conditions but also are often thought of as solid-lubricant materials. Polymers' ability to provide reasonably low friction coefficients and wear rates under a wide range of working conditions with high reliability have made them a widely used material for dry or self-lubricating bearings and bushings. As a class of materials, polymers typically have large ratios of strength to modulus and low surface energies; these attributes help mitigate wear by promoting large elastic strains and by facilitating the transfer of protective films to high-energy surfaces, respectively.

Ultrahigh-molecular-weight polyethylene (UHMWPe) is a unique polymer solid lubricant in that it exhibits relatively low friction and wear without lubricating or reinforcing fillers. Its most notable tribological application is as the bearing material in orthopedic devices; in boundary-lubricated unidirectional conditions with water or bovine serum, friction coefficients are on the order of 0.05 (120), and wear rates approach 10^{-9} $mm^3/(N{\cdot}m)$ (121), a value rivaled by mass gains from fluid uptake. Its unidirectional wear rate is roughly two orders of magnitude lower than that found in vivo, however. During sliding, traction forces reorient the polymer chains at the surface, which significantly strengthens the material and reduces wear rates (121). Joint kinematics studies have revealed significant deviations from linear sliding (122), and cross-shear from controlled, multidirectional sliding increases friction by 100% (120) and wear to values more consistent with those found in vivo (121).

Other polymers exhibit significantly higher friction or wear than UHMWPe under most conditions and require the addition of lubricating or reinforcing fillers (123). Lancaster (124) was among the first to investigate fiber reinforcement as a route to improve friction and wear properties of polymers. The addition of 30% high-strength carbon fibers reduced friction by 50% and reduced wear by more than 90% for all but four already wear-resistant polymers. Follow-up studies showed that perpendicularly oriented fibers produced the greatest reinforcement effect and proposed that the perpendicular orientation maximized preferential load support by the filler. Sung & Suh (125) made similar experimental observations but proposed that the perpendicular orientation interfered with the propagation of subsurface cracks.

PTFE, perhaps the most notable tribological polymer due to its exceptional frictional properties, has shown the greatest capacity for wear reduction through filler reinforcement. Although the highest reported wear rates among polymers belong to unfilled PTFE (126), the lowest reported wear rates belong to a PTFE-based composite (127). Tanaka et al. (128) first attributed the unusually high wear rate of PTFE to the ease of destruction of its unique banded structure. Bahadur & Tabor (129) found that effective fillers reduced the size of the wear debris, which more readily attached to the countersurface to form a protective transfer film that helps prevent

subsequent wear. Blanchet & Kennedy (130) showed that the wear rate of PTFE was unusually high only above a critical speed and determined that the transition occurred when frictional shear stresses exceeded the interfacial strength of subsurface cracks. They proposed that fillers reduced wear rates of PTFE by interrupting subsurface crack propagation.

Tanaka & Kawakami (131) were the first to investigate the effect of filler size on wear reduction of PTFE composites. The filler that provided the poorest improvement in wear resistance was TiO_2, which happened to be the only nanoscale filler in the study. This result was consistent with the crack interruption and preferential load support hypotheses; Tanaka & Kawakami concluded that small particles cannot effectively prevent the destruction of the banded structure and are simply swept away within large debris particles. At this time, the community agreed that nanoscale fillers were unable to reinforce polymeric solid lubricants.

In the late 1990s to 2000, Wang and colleagues (132–136) published a series of papers on the reinforcing effects of ceramic nanofillers on polyetheretherketone (PEEK). Although PEEK is already quite wear resistant without reinforcement, nanofillers reduced wear by as much as 10 times [down to 10^{-6} mm^3/(N·m)]. The first PTFE nanocomposite study since the initial report by Tanaka & Kawakami (131) was published by Li et al. (137) in 2001 on nanoscale ZnO-reinforced PTFE. Li et al. showed reductions in wear from 10^{-3} mm^3/(N·m) to 10^{-5} mm^3/(N·m), but perhaps the most important result was the deterioration of wear resistance beyond an optimum loading, an observation that conflicts with the prevailing linear-rule-of-mixtures models. In 2003, Chen et al. (138) showed that carbon nanotubes reduced wear further to 2×10^{-6} mm^3/(N·m). Although this improved effect from large-aspect-ratio fillers was consistent with the hypotheses of the time, a 2003 study by Sawyer et al. (139) showed that alumina nanoparticles provided further reductions at lower filler loadings [1×10^{-6} mm^3/(N·m) at 10%]. In 2005, Burris & Sawyer (140) published a study of roughness effects on the wear of the alumina-PTFE nanocomposite. By varying the filler particle size in an attempt to study the interaction between asperity height and particle radius, they discovered that the larger alumina particles reduced wear by another order of magnitude at loadings as low as 1 wt%. Later studies showed that trace (<1%) nanofillers could reduce steady-state wear rates to less than 10^{-7} mm^3/(N·m), nearly four orders of magnitude below the rates for unfilled PTFE (141). Independent follow-up studies corroborated the unusually low wear rates of these materials and changed the landscape for the design of polymeric tribomaterials (142–145). These PTFE-alumina nanocomposites with steady-state wear rates of $\sim 10^{-7}$ mm^3/(N·m) and less are referred to as ultralow-wear PTFE composites.

3.2. Nanoscale Interactions Offer New Direct-Reinforcement Mechanisms

Traditional polymer composites use high loadings (20–50%) of hard, perpendicularly oriented fillers to enhance wear performance through well-understood mechanical routes (**Figure 7*a***). Unfortunately, these characteristics sacrifice other (e.g., ductility, thermal, and chemical) properties of the polymer while abrading transfer films and the countersurface and thus partially offset their reinforcement effects. Initially, nanoparticles may have been proposed to address the abrasion problem, as nanoparticles have a characteristic dimension (<200 nm) smaller than the transfer film thickness. However, nanoparticles can be extremely hard, and nanoparticle abrasion can polish the countersurface to promote transfer film stability. Furthermore, nanoparticles have high number densities and ratios of surface area to volume. A nanocomposite has one thousand times the filler surface area and one billion times the number of particles of a comparable microcomposite (i.e., 20-nm versus 20-μm average filler diameter). Although polymers and fillers are often inert and are expected to have weak interfaces, the likelihood for chemical interaction increases with an increased ratio of surface area to volume.

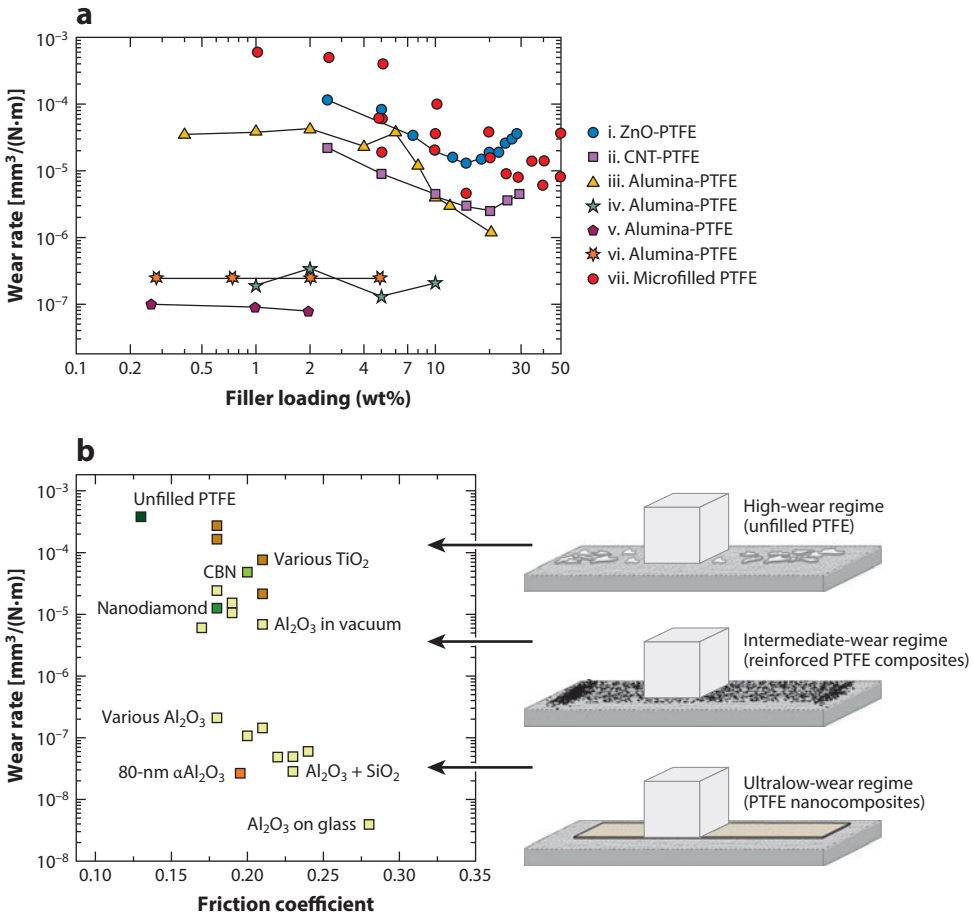

Figure 7

(*a*) Wear rate versus filler weight percent for PTFE microcomposites and nanocomposites in the literature: (*i*) Reference 137, (*ii*) Reference 138, (*iii*) Reference 139, (*iv*) Reference 146, (*v*) Reference 141, (*vi*) Reference 144, and (*vii*) References 147–151. (*b*) Steady-state wear rate versus average friction coefficient for PTFE filled at 5 wt% with various fillers sliding against stainless steel at 250-N normal load, 50.8-mm/s sliding speed, and 25.4-mm stroke length. Abbreviation: CNT, carbon nanotube.

Numerous investigators have found significant improvements in mechanical properties of a range of polymers with low loadings of nanofillers (152–164). Eitan et al. (153) found significant load transfer across the interfaces of multiwall carbon nanotubes and polycarbonate using Raman spectroscopy; the degree of load transfer increased when nanotubes were treated. Low loadings of nanofillers also dramatically change glass transition temperatures, the crystalline phase, and the morphology of the polymer (158, 165–169). Contrary to the traditional view of mechanical reinforcement, in which the filler and polymer behave as they would individually, these results suggest that these fillers can fundamentally change the polymer.

Physical interactions at the polymer/filler interface have long-range effects on the polymer over a nanoscale region known as the interface region, the interaction zone, or the interphase. Maiti & Bhowmick (170) used atomic force microscopy to show that the thickness of the interface region is on the nanometer length scale and increases with compatibility between the filler and the matrix.

Although the effects of a nanoscale interface region on a traditional composite are negligible, these regions can make up a significant fraction of the total volume of a nanocomposite, resulting in dramatic changes in the apparent properties of the polymer.

3.2.1. Potential effects of the interface region on the wear of PTFE nanocomposites. One interesting insight into the origin of ultralow-wear PTFE composites is that, with otherwise identical conditions, the mechanism can be switched on or off by changing the alumina nanoparticle (140). This insight suggests that some physical or chemical property of the particle, and more specifically of the particle surface, activates the mechanism. We consistently find that low-wear PTFE fibrillates extensively, particularly near stress concentrators, whereas high-wear PTFE blunts and ruptures. These stark mechanical differences suggest that the particles fundamentally change the polymer.

The mechanical properties of PTFE depend strongly on its crystallinity, crystalline phase, and crystalline morphology (171–175), all of which may be strongly influenced by interactions at the polymer/nanoparticle interface. PTFE has a unique crystalline structure that is often described as banded, and this banded structure contains intermittent bands of crystalline polymer and amorphous polymer (128); the viscoelastic properties of this banded structure are related to its friction and wear responses (176). Within crystalline regions, lamellar slices are composed of folded PTFE chains. An individual chain is a fully fluorinated carbon backbone in a helical conformation, the twist of which dictates the phase. The three well-known phases occur near room temperature. Phase II (177, 178) exists at less than 19°C, is the most brittle phase, and is characterized by a triclinic unit cell with $a = b = 0.559$ nm. Phase IV exists between 19 and 30°C; as temperature increases beyond 19°C, the helix untwists, the lattice becomes hexagonal, and the lattice spacing increases by ∼1% (177). Phase I, which exists at greater than 30°C (179), is the toughest phase (173) and is characterized by a distorted hexagonal lattice and by general molecular disorder (180–182).

Preliminary differential scanning calorimetry (DSC) and XRD measurements were made to investigate whether nanoparticle stabilization of the tough phase I contributes to wear reductions of these low-wear materials (183). Initial low-temperature DSC suggested that α-phase alumina (α alumina) reduced the PTFE phase-transition temperatures (I–IV and IV–II) by ∼2°C, which suggests increased molecular disorder at a given temperature. Room temperature XRD produced consistent results. The full-width half-maximum of the primary peak ($2\theta = 18°$) increased, whereas the magnitude of 2θ at the peak decreased; these results indicate increased deviation of the lattice spacing and increased mean lattice spacing, respectively. The peak height in the $2\theta = 35$–$45°$ region was reduced relative to the background, suggesting increased deviations in the helix conformation (along each chain or from chain to chain). High-temperature DSC showed increased crystallinity and melt temperature (by 1°C at 5 wt%); these results suggest that nanoparticles may have helped nucleate crystallization and increased the size or organization of the crystals, respectively. However, more recent and exhaustive, unpublished studies have shown that such changes do not always occur, nor do they correlate to the wear resistance of the material. PTFE is an extremely complex semicrystalline polymer, and although no definitive signature of wear resistance has yet been identified with standard polymer characterization techniques, there is no doubt that the ultralow wear rates observed are made possible by one or more nanoscale phenomena.

3.2.2. Dispersion. The influence of the nanoparticles on the polymer is limited by how well the particles have been dispersed. High surface area per unit volume, the very property that makes nanoparticles special, also encourages them to stick or agglomerate. This behavior results in a competition between the potential for mechanical enhancement and difficulty of dispersion. Such

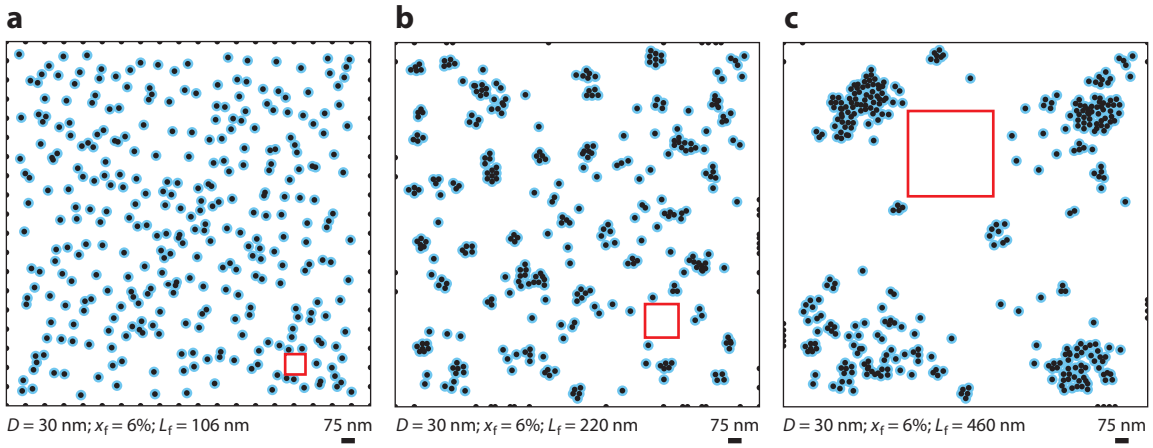

Figure 8

Schematic illustrations of the effects of nanoparticle dispersion on the free-space length L_f for a 6% nanocomposite; the dispersion quality deteriorates, and L_f increases from left (*a*) to right (*c*). The polymer is shown in white, the nanoparticle is shown in black, and the interface region is shown in blue at the interface of the particle and the polymer. Red boxes represent the free-space length of each dispersion.

limitations may have played a role in the poor performance of early nanocomposites, particularly those involving high loadings of particles (10–50%). Comparisons between studies have been difficult due to the lack of a standard quantitative dispersion characterization method. Although many proposed methods (184–194) characterize a property of the distribution of particles (a strategy with virtually endless possibilities), our experience with tribological nanocomposites suggests that the characteristic size of the unreinforced polymer domain is the feature that matters most; we have termed this the free-space length, L_f (195). As L_f decreases, the influence of the interface region (**Figure 8**) increases along with the reinforcement effect. We would therefore expect smaller, better dispersed, and higher loadings of fillers to improve the properties. **Figure 8** illustrates the effect of dispersion quality on L_f for a 6% nanocomposite.

To investigate the role of dispersion, a fluorinated silane treatment (trifluoropropyl trimethoxysilane) was used to improve the dispersibility of α alumina in PTFE (141). Wear rates were measured at 0.125, 0.5, and 1% loadings with treated and untreated nanoparticles. Wear rates of untreated nanocomposites were low at higher loadings but became inconsistent at 0.125% loadings, reaching 10^{-4} $mm^3/(N{\cdot}m)$ in one case. Low and stable wear rates were found for each treated sample. Although agglomerates were observed in both cases, untreated nanoparticles were always clustered, whereas treated nanoparticles were found individually and clustered; the result was a reduction in L_f from 1,240 to 540 nm.

Although there remain many open questions about the specific mechanisms that enable trace loadings of particles to reduce polymer wear by four orders of magnitude, the literature suggests that nanoscale fillers (with high ratios of surface area to volume), quality filler dispersions, and strong interactions between the polymer and filler are favorable. The α alumina appears to be particularly effective at low loadings, especially under enhanced dispersion conditions, for reasons that likely involve uncharacterized long-range effects of the particle/polymer interface on the nearby polymer chains. Numerous other fillers also promote ultralow wear in PTFE, although many others do not. Successful PTFE nanocomposites have exhibited the tendency to fibrillate during failure. The results suggest that the dominant mechanisms of reinforcement are damage localization

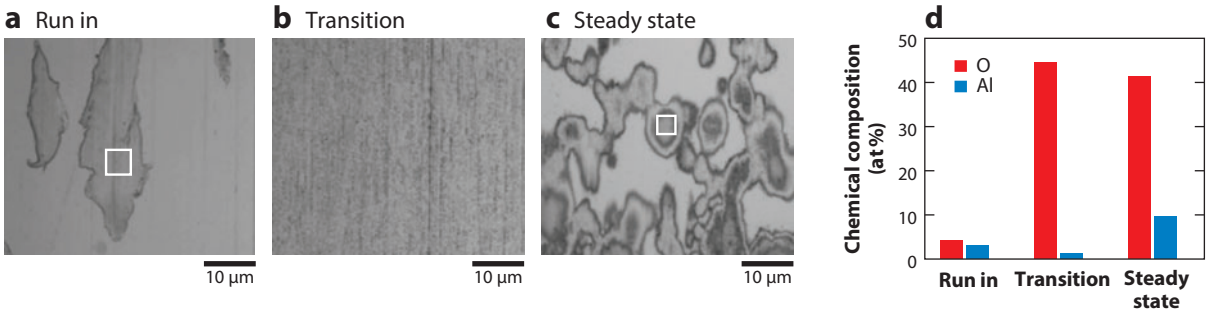

Figure 9

(*a–c*) Images showing transfer film's characteristic morphology in the (*a*) run-in, (*b*) transition, and (*c*) steady-state phases. (*d*) Energy-dispersive spectroscopy analysis showing the relative concentrations of O and Al at the run-in and steady-state stages, which correspond to the locations on the surfaces delineated by the white boxes in panels *a* and c. The Al reflects filler contributions, whereas the O reflects defluorination and oxidation of the PTFE.

[interruption of crack propagation (130)] and the corresponding regulation of debris size (129), which encourages the adhesion of the protective transfer films necessary for low-wear sliding.

3.3. Mechanisms of Secondary Reinforcement Through Transfer Films and Tribofilms

Polymer composites are often mated against a relatively smooth and hard countersurface. Once debris particles are removed from the composite surface, they stick to the countersurface, transfer back to the composite, or escape the tribosystem altogether. The material that transfers to the countersurface becomes a protective layer termed the transfer film. In general, when materials slide with low and ultralow wear rates, they produce fine wear debris and thin, uniform transfer films. This observation has led to the widely held belief that fine wear debris and high-quality transfer films play critical roles in wear reduction.

3.3.1. Debris size, transfer film morphology, and relationship with wear. These ultralow-wear PTFE nanocomposites endure a run-in period of elevated wear rates before transitioning to ultralow wear at steady state. We recently conducted in situ studies of the transfer film to investigate how it forms and the role it plays in the transition to ultralow-wear sliding (196). We observed three distinct transfer film morphologies (**Figure 9**). In the run-in phase, high wear rates were accompanied by the deposition of relatively large platelets onto the countersurface. As sliding continued, the size of the platelets and the wear rate monotonically decreased, but interestingly, the platelets were removed and replaced on a cycle-by-cycle basis throughout the run-in phase. These results indicate that transfer film adhesion is initially uninvolved and refute the hypothesis that the nanoparticles serve primarily to directly bond the polymer debris to the counterface. Energy-dispersive spectroscopy (EDS) of the transferred material showed that the composition was identical to the bulk material, a result that refutes the hypothesis that (at least without other inputs) the particles degrade the polymer to promote adhesion.

The debris size decreased with sliding until no new debris were observed; this point marks a transition period for which cycle-by-cycle wear was immeasurable (to 10 μg) and any transferred debris became optically undetectable. With continued sliding, the region darkened optically, and scanning electron microscopy revealed that the darkening was due to the accumulation of nanoscale

PTFE fragments (~100 nm in lateral dimension) that were alumina deficient and heavily oxidized. With further sliding, these deposits became optically visible and persisted for, as far as we could tell, the remainder of the experiment. Clearly, these fragments were strongly adhered, possibly because degradation offered the opportunity for strong bonding or because the energetics of the small size scale favored adhesion over removal (probably both). We term these fragments seeds because they appear to nucleate the growth of the transfer film in its traditional embodiment (196).

Following a period of sliding in the transition phase, the sudden occurrence of a significant wear event produced optically visible debris fragments and a quantifiable change in mass. These larger wear fragments also adhered for extended periods of sliding, suggesting degradation-enhanced adhesion. With continued sliding, existing fragments coalesced, and additional fragments were deposited to eventually form a continuous network, as shown in **Figure 9**. During the steady-state phase of wear, the transfer film was worn and new wear fragments were deposited at equal rates. EDS showed that the steady-state films were heavily oxidized and alumina rich.

3.3.2. The tribochemistry of ultralow-wear PTFE composites. Whereas EDS can provide compositional clues into filler accumulation and oxidation, X-ray photoelectron spectroscopy (XPS) can be used to probe specific chemistries. XPS measurements revealed evidence of a new chemical species in tribofilms (an altered "skin" on the surface of the worn polymer composite) and in transfer films following ultralow-wear sliding (**Figure 10**). The new peaks in the C 1*s* spectrum are consistent with defluorinated and otherwise degraded PTFE. XPS suggests that the tribochemically generated species observed in the transfer film of ultralow-wear alumina-PTFE composites is consistent with oxygen-containing end groups that were not present before sliding. It is hypothesized that this new species enhances transfer film adhesion. The formation of these new end groups requires defluorination or backbone cleavage (to provide a reaction site) and sources of oxygen and/or either water or hydroxide near the sliding interface; in laboratory experiments, humid air can provide both. This hypothesis suggests that the wear performance of these systems depends strongly on the environment.

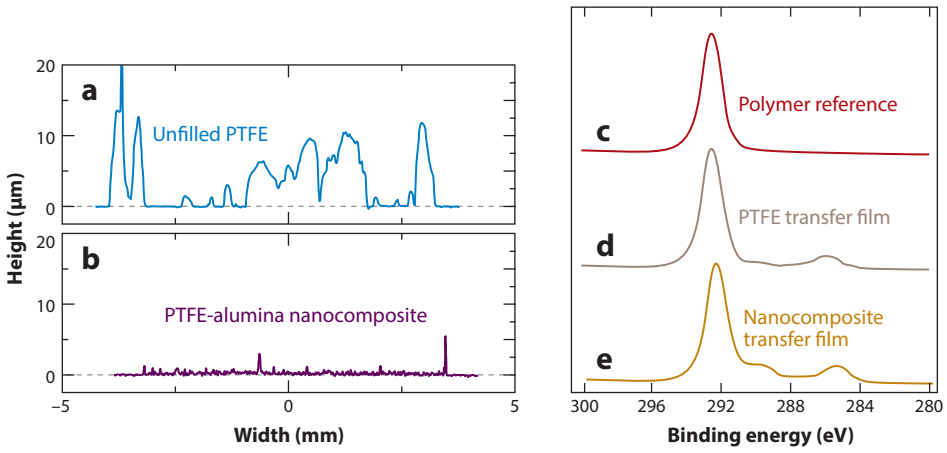

Figure 10

(*a*) Unfilled PTFE and (*b*) PTFE nanocomposite transfer film topography as formed by sliding against a 304L stainless steel countersample. (*c–e*) C 1*s* X-ray photoelectron spectra for (*c*) an unfilled PTFE reference sample, (*d*) an unfilled PTFE transfer film, and (*e*) a PTFE and 5-wt% alumina nanocomposite transfer film formed on stainless steel in an environment of N_2 (~80%) and O_2 (~20%) with a relative humidity of ~35%. From Reference 145.

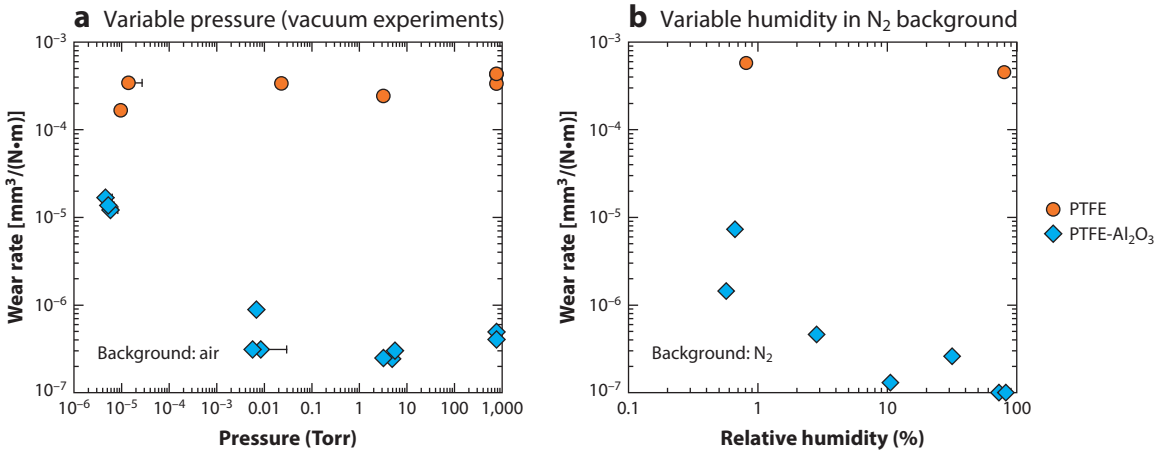

Figure 11

Wear rate as a function of (*a*) water partial pressure and (*b*) relative humidity for a PTFE composite filled with 5-wt% α alumina and slid against stainless steel at 250-N normal load, 50.8-mm/s sliding speed, and 25.4-mm stroke length. From References 145 and 197.

Experiments were performed in air (80% N_2/20% O_2), humid nitrogen (145), and humid vacuum environments (197). Wear rate is plotted as a function of chamber pressure and relative humidity in panels *a* and *b* of **Figure 11**, respectively. The wear rate of the PTFE-alumina nanocomposites increased with decreased environmental water vapor, whereas the wear rate of unfilled PTFE did not (**Figure 11**). These wear experiments in various environments support the hypothesis that tribochemistry between the worn samples and the environment plays an important role in wear reduction.

3.3.3. Tribological bond breaking. Contrary to the predominant delamination wear mechanism and the notion that PTFE exhibits poor adhesion, several investigators have shown that extremely thin and oriented fragments of PTFE transfer readily and adhere strongly. Our recent in situ surface plasmon resonance tribology experiments supported these results and showed that PTFE transfers as early as the first cycle (198). XRD and atomic force microscopy studies of PTFE transfer films have shown molecular alignment and structure consistent with the drawing of individual chains (or small collections) from the bulk. Such transfer requires that chains (typically 10–100 μm in length) be drawn completely from the entangled bulk or be broken (chain scission) when the draw stresses exceed the strength of the backbone. If we assume that the C-C bond and PTFE-countersurface bond (through van der Waals interactions) have characteristic strengths of 1 GPa and 10 MPa, respectively, a simple force balance predicts that the chain breaks when it interacts with the countersurface over a length of >50 nm. This estimate suggests that chain scission is actually quite favorable, explains observations of immediate transfer, and offers the pathway for tribochemical reaction and strong adhesion.

The notion of tribochemistry (199), including chain scission and reaction, has been explored in fluoropolymers (200–210). Using a computational chemistry approach, Onodera et al. (210) showed that PTFE can be defluorinated by alumina to form a carbon radical, which can interact with the environment and other surfaces. The possible tribochemical defluorination of PTFE and other fluoropolymers has been identified through Auger spectroscopy and XPS (201–205, 207). Other researchers show possible mechanisms for transfer film formation caused by enhanced tribochemical interactions and chain scission (206, 208–210). Combining the

mechanistic possibilities (206, 208–210) with the results from the environmental experiments (145, 197) clarifies the tribochemical mechanisms. Chain scission event sites, when terminated by constituents from water, promote the formation of carboxylates (206). Numerous C-C bonds are broken each time a wear particle is generated, providing abundant opportunities for chemistry and unique new tribological surfaces, which is likely why the friction coefficient of PTFE-alumina composites increases to values of 0.15 to 0.2 or greater as the transfer film reaches a steady state.

3.3.4. Tribofilms. Although a well-adhered transfer film is necessary for ultralow wear, the formation of a robust tribofilm on the polymer surface is perhaps of equal importance (211). Interestingly, initial wear rates at early sliding cycles are comparable for unfilled PTFE and PTFE-alumina composites (**Figure 12**); here, unfilled PTFE and 2-, 5-, and 8-wt% alumina–filled PTFE

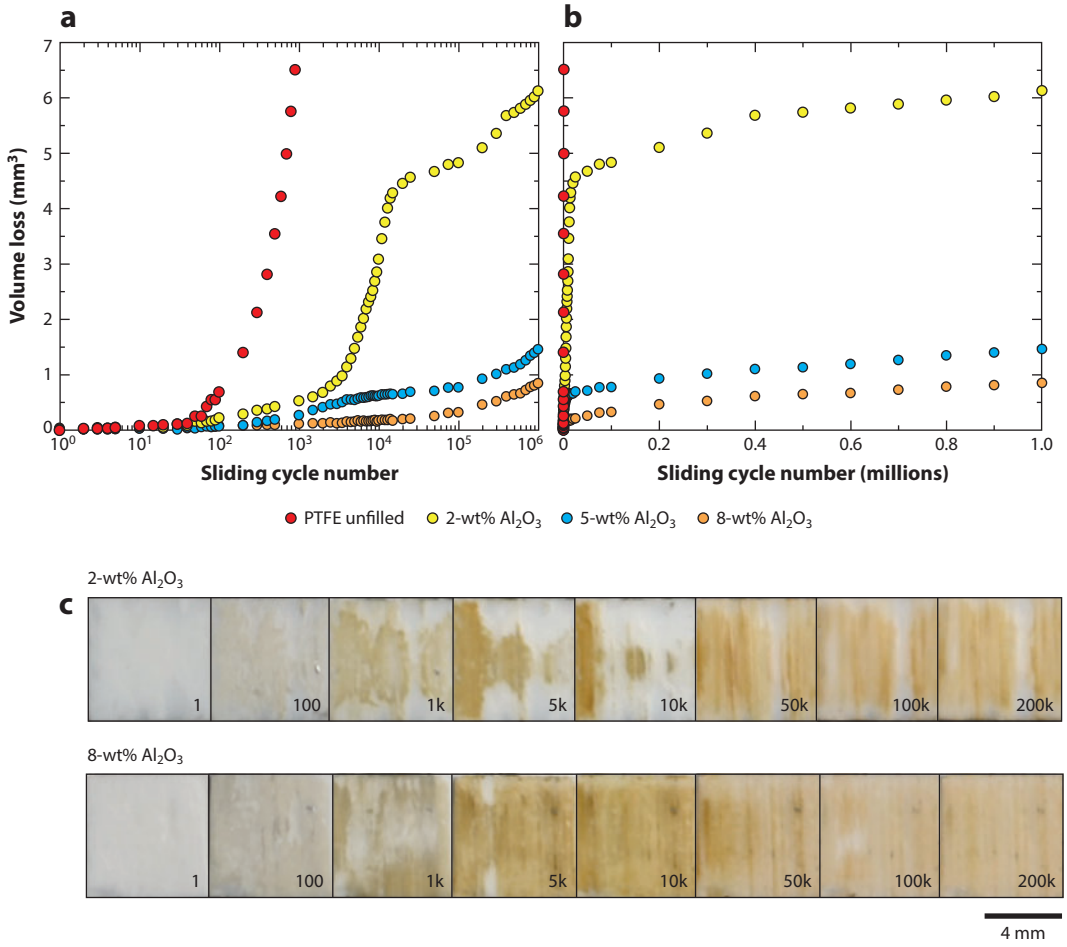

Figure 12

(*a*,*b*) Run-in and tribofilm formation. Total volume lost as a function of sliding cycle for unfilled and 2-, 5-, and 8-wt% α alumina–filled PTFE composites slid against stainless steel at 250-N normal load, 50.8-mm/s sliding speed, and 25.4-mm stroke length. Plotted on (*a*) semilog and (*b*) linear axes for visualization. (*c*) Images of tribofilms on the wear surface of the polymer composite for 2- and 8-wt% α alumina composites. Cycle number is shown at the bottom-right of each image in panel *c*.

composites are slid against a stainless steel countersurface. When wear volume is plotted as a function of sliding cycle (or time or distance), there is a transition from an initial high wear rate to an ultralow wear rate. The transition from high wear to low wear occurs earlier with increasing filler loading percent (up to 8 wt%). The dispersion quality of these samples would be classified as poor to moderate by most standards (211). In this case, the poor dispersion can be supplemented by increased filler loading. This finding suggests that low wear requires a critical loading of filler for sufficient damage compartmentalization.

The transition from high wear to ultralow wear during the initial sliding, or run-in period, of PTFE-alumina composites also coincides with the development of a brown tribofilm on the surface of the polymer composite (**Figure 12*c***) (211). This tribofilm is more readily formed with increased filler loading up to 8-wt% alumina filler. The 8-wt% alumina composite readily forms a tribofilm after ∼1,000 to 5,000 sliding cycles (**Figure 12*c***) and very quickly transitions to an ultralow, steady-state wearing system. However, the 2-wt% alumina composite takes much longer to form a steady-state film (**Figure 12*c***), which corresponds to a longer run-in period. There is also a period during which the tribofilm starts to form (at approximately cycle 1,000) and then subsequently wears (cycle 5,000 to 10,000), corresponding to extended high wear rate. A stable tribofilm is formed between cycle 10,000 and cycle 50,000 (**Figure 12*c***), and the system transitions to ultralow wear at approximately cycle 20,000 (**Figure 12*a*,*b***). After extended sliding cycles (hundreds of thousands to millions of sliding cycles), ultralow, steady-state wear is reached [as low as 2×10^{-8} $mm^3/(N \cdot m)$]. For perspective, this wear rate equates to one monolayer of PTFE being removed from the surface every 100 sliding cycles (although in reality wear and transfer events are much larger and infrequent).

XPS analyses of the tribofilm revealed tribochemically degraded PTFE as shown in **Figure 10** (145). Furthermore, nanoindentation revealed that this tribofilm on the wear surface of the polymer is mechanically harder and stiffer than the bulk composite and unfilled PTFE; in fact, the tribofilm is progressively harder with increased sliding cycles (211). This increase in hardness is consistent with the increased hardness of degraded PTFE and with the accumulation of hard nanoparticles at the tribological interface. The tribochemically degraded PTFE in the tribofilm may have improved cohesive strength, may better regulate debris size through crack arresting, and may replenish transfer film with new carboxyl-terminated debris.

3.4. Summary

We have found that trace quantities of nanofillers can reduce the wear of PTFE by four to five orders of magnitude, an improvement that cannot be explained through traditional reinforcement mechanisms. We have worked to elucidate the responsible mechanisms for nearly a decade and have found a number of potential contributing factors. Although we have not pinpointed exact mechanisms, they appear to be nanoscale in nature and to feedback into one another. **Figure 13** illustrates our current hypothesis for the unprecedented dry-sliding wear performance of these unique nanocomposite materials.

Low loadings of well-dispersed nanoscale fillers maximize the interaction area between the filler and the matrix and minimize the characteristic length scale of the unreinforced polymer. These interactions, when sufficiently strong, may have long-range effects on the polymer and on its mechanical response at the nano-, micro-, and macroscales. Interestingly, wear rates, debris morphology, and transfer film properties are relatively unaffected by the particles during the early stages of sliding, which suggests that the reinforcement effect is primarily indirect. Debris are initially compositionally identical to the bulk and do not adhere to the countersurface (**Figure 13*a***). The wear rate and debris size of all PTFE nanocomposites decrease with continued

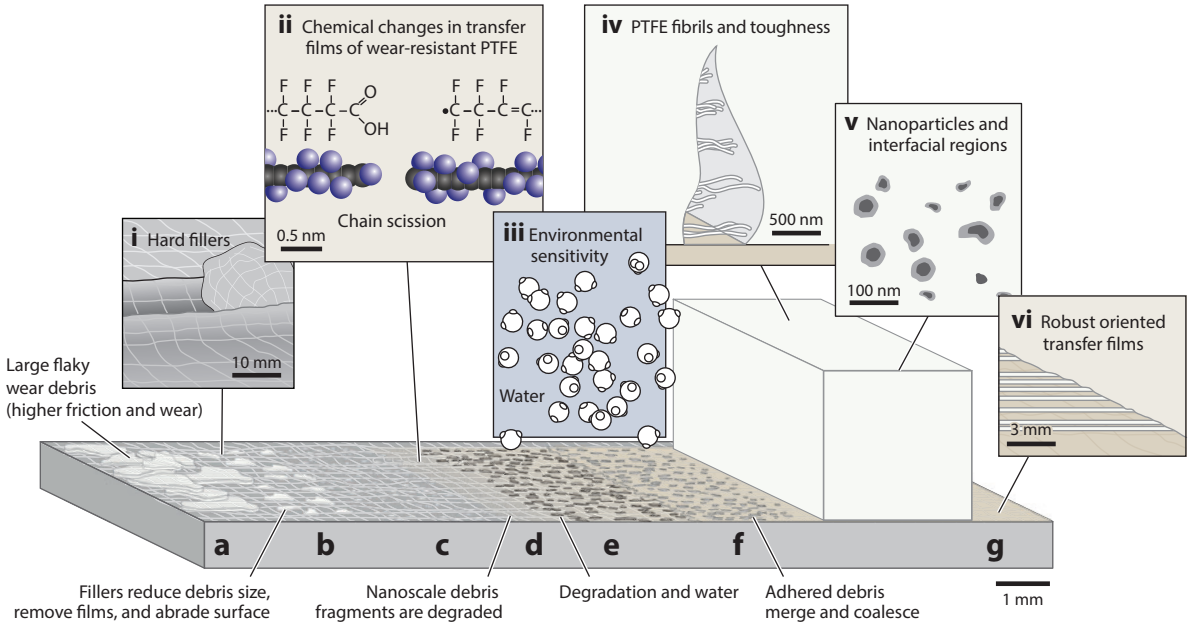

Figure 13

Mechanistic hypothesis for ultralow-wear PTFE nanocomposites. Characteristic processes of transfer film formation are illustrated in relative order from *a* through *g*. Notable observations and interactions are described in *i–vi*.

sliding (**Figure 13*b*,*c***), but only ultralow-wear PTFE exhibits marked degradation at the interface (**Figure 13*d***). These chemical modifications lead to harder, more brittle (possibly through cross-linking and conjugation), and more-wear-resistant polymer surfaces. We can disrupt ultralow wear by removing the environmental water vapor necessary to form the chelating reaction products, supporting the importance of tribochemistry. The nanoparticles may reduce the barriers to PTFE defluorination and chain scission to promote this tribochemistry.

Whereas debris size and wear rates reach moderate steady-state values, the wear rates of ultralow-wear materials continue to decrease until debris become optically undetectable (**Figure 13*d***). At this point, chemically degraded nanoscale PTFE fragments transfer and strongly adhere to the countersurface; nanoscale phenomena are likely involved in accelerating reactions and increasing adhesive strength. During the transition phase, frictional input continues to chemically and mechanically degrade the surfaces until the first significant posttransition wear event occurs (**Figure 13*e***). Unlike debris from the run-in phase, debris from the steady-state phase degrade, adhere strongly to the countersurface, and coalesce (**Figure 13*f***) to form a continuous and stable transfer film (**Figure 13*g***) that is eventually worn and replenished at equal rates.

Although nanofillers typically improve mechanical properties only modestly, we have shown that trace quantities of nanofillers can increase the wear resistance of a polymer by 10,000 times; to our knowledge, this is the most extreme example of nanofiller reinforcement in the polymer nanocomposites literature. The model we describe here remains a hypothesis but is consistent with nearly a decade of work by our group and others in the field to elucidate the responsible mechanisms. Although the specific nanoparticle surface property responsible for activating the ultralow-wear mechanism in PTFE has not been isolated, the observation that wear resistance can

be switched on and off with only subtle filler changes has exciting implications for the future of tribomaterials design and for other areas of polymer science and engineering.

4. IONIC SOLIDS

The usefulness of ceramics as tribological materials is evident in theory and in practice (212, 213) [e.g., in the context of gas turbine engine bearings (213)]. Ceramics are found in a wide range of engineering applications in the form of both thin films and bulk materials due to their superior wear resistance, hardness, fatigue strength, thermal stability, and chemical inertness compared with conventional metal alloy materials. Erdemir considered the ionic potentials of crystalline oxides to select bulk (214) and design nanocomposite (215) solid-lubricant materials. Later, a data-driven, informatics approach was used to predict friction coefficients of single-crystal ionic solids on the basis of a range of materials parameters, including electronegativity, intermolecular distance, Madelung constants, melting temperature, density, and numerous other parameters (216). However, a fundamental understanding of the mechanisms of friction and wear remains elusive, largely due to the complex dynamic and transient nature of tribological systems. The availability of tribometers with high-resolution in situ microscopy (217) is rapidly bridging the gap between idealized physical systems and practical experiments and is enabling more sophisticated experiments in attempts to understand the tribological behavior of ceramics in varying environments at the single-asperity scale.

More generally, single-crystal ionic solids, which naturally span several orders of magnitude in wear resistance, offer a unique opportunity to understand and characterize the structure-function relationship for the fundamental mechanisms of energy dissipation in sliding interfaces that result in wear and friction.

With the advent of friction force microscopy (218), tribological interactions between materials can be made at the atomic scale, revealing new frictional and wear behaviors (219–228). Crystalline ionic solids and minerals have revealed remarkable behavior at the nano- and atomic length scales, including direction-dependent friction (229), site-specific friction (terrace versus step sites) (228), atomic stick slip (221, 223, 227), velocity-dependent friction (225), and thermally activated friction and wear (224). Modeling and simulation efforts to explain the tribological phenomena observed in these systems include various Tomlinson models (230–233), atomistic calculations (234, 235), and MD simulations (19, 236, 237).

Remarkably, in the 1960s fundamental observations were made to link macroscale friction experiments to atomic structure of ionic solids, prior to the capabilities of molecular simulations and nanoscale experiments. In 1964, Steijn (238) and Bowden et al. (239) first observed crystallographic orientation dependence on the coefficient of friction of single-crystalline, ordered solids, including rock salts, diamond, and face-centered-cubic and body-centered-cubic metals. Both Steijn and Bowden et al. performed experiments on the same {001} family of planes of the rock salt structure; **Figure 14** shows the result of the anisotropy in friction for Steijn's NaCl experiment (**Figure 14*a***) and for Bowden et al.'s MgO experiment (**Figure 14*b***). These studies were among the first to link molecular order and orientation to tribological properties. More recently, motivated by a renewed interest in the tribological behavior of ceramics at high temperatures, Erdemir (240) investigated the friction behavior of various self-mated oxides and composite oxide materials at temperatures in the range of 300–1,200 K and proposed a general correlation between high ionic potentials and highly screened cations with low-friction behavior.

Interestingly, Steijn (238) and Bowden et al. (239) showed opposite trends in friction coefficient dependence on sliding direction. Bowden et al. reported the highest friction in the <100> family of directions, and Steijn showed high friction in the <110> family of directions. Several differences in

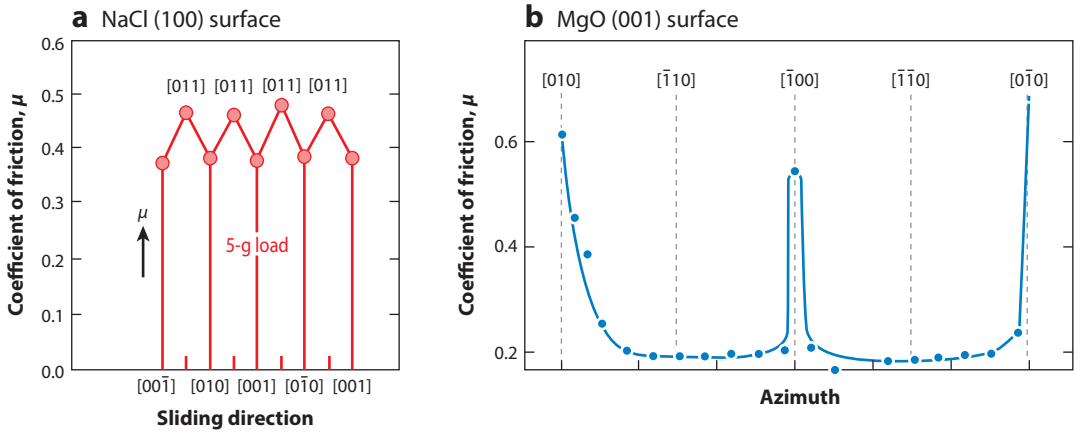

Figure 14

Frictional anisotropy in crystalline solids. (*a*) Coefficient of friction on the (100) surface of NaCl as a function of crystalline sliding direction as presented by Steijn (238). The *x*-axis sweeps through 360° of sliding directions. (*b*) Coefficient of friction on the (001) surface of MgO as a function of crystalline sliding direction as reported by Bowden et al. (239). The *x*-axis sweeps through 180° of sliding directions. Both experiments are on the same {001} family of planes of the rock salt structure.

the experiments may account for this disagreement. First, MgO and NaCl have different properties due to the relative charges of each (+2:−2 versus +1:−1, respectively). Additionally, the loading conditions (contact stresses and stress distributions) and probe materials differed: Bowden et al. used sharp conical diamond probes, whereas Steijn used 1/16-inch-diameter sapphire probes. Unlike Bowden et al., Steijn reported no measurable variation in friction of MgO for the sapphire spherical probes at comparable loads. This difference in contact pressure and contact geometry resulted in higher contributions of plowing friction in the measurements on MgO by Bowden

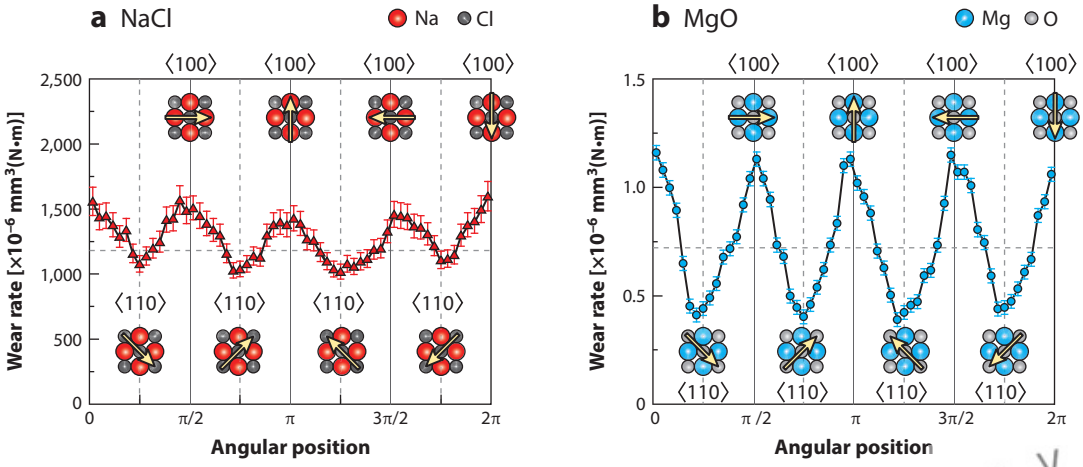

Figure 15

Wear anisotropy in crystalline solids. Wear rate on the (100) surface of (*a*) NaCl and (*b*) MgO as a function of crystalline sliding direction. The *x*-axis sweeps through 360° of sliding directions.

et al. In contrast, the sliding experiments on NaCl by Steijn resulted in a more gradual material removal process, with adhesive interaction and plastic flow dominating the frictional anisotropies.

Fifty years later, we present a comparable experiment that links the wear rate of a rock salt to the crystalline order and orientation (**Figure 15**). Wear experiments on the (001) surface of rock salts, including NaCl and MgO, revealed that the materials wear rates have a significant dependence on crystallographic wear direction. These wear experiments used a 1/8-inch-diameter sapphire ball with an applied normal load of 1 N. The materials experienced maximum wear when sliding in the <100> family of directions and minimum wear when sliding in the <110> direction. For MgO, the wear rate in the <100> direction was approximately three times higher than in the <110> direction. These trends are strikingly similar to the friction results provided by Bowden et al. (239) as well as by Steijn (238) in 1964. This new link is made possible by advances made in instrumentation and technologies that are available to modern scientists. Five decades ago, Steijn and Bowden et al. noted that the wear tracks were wider in the <100> family of directions than in the <110> family of directions for materials such as NaCl, LiF, and MgO. These findings not only provide a link between materials structure and property but highlight the importance of a material's short- and long-range order, organization, and orientation in relation to its tribological properties. These new results provide insight into the molecular origins of wear and present the opportunity to predict and design ionic solids for ultralow-wear operation. Furthermore, the dependence of wear on sliding direction of these materials suggests that systems can be further optimized for low wear by orienting materials and coatings for optimal wear performance.

5. CLOSING REMARKS

More than five centuries after da Vinci's pioneering work, the study of friction and wear of bulk materials remains a practically relevant and scientifically fruitful endeavor. The tables of friction and wear properties commonly found in design textbooks belie the true complexity of tribological contacts. Theoretical modeling and nanoscale experimentation have shown that friction is fundamentally driven by intermolecular forces. The macroscopic friction coefficients and wear rates expressed by single-crystal ionic solids, for example, reflect the roles of crystallographic orientation and bond energy of the surface ions. Additionally, even molecularly thin films of adsorbed species from the environment can dramatically change the nature of the surface interactions. For metals, the removal of adventitious carbon or other environmental contaminants can lead to direct metal-to-metal contact, strong adhesion, order-of-magnitude-increased friction, and several-orders-of-magnitude-increased wear.

Wear events are highly irregular, making controlled and systematic experimental studies of the underlying fundamental processes challenging. The integration of high-resolution in situ characterization methods is opening new pathways for fundamental investigation. Intermolecular forces are short ranged and exist only at locations of intimate contact. These real contact areas are typically much smaller than the apparent area, occur only at the most prominent opposing asperities, and rapidly change locations as sliding ensues. When bonds are broken through wear, the environmental species tend to dictate the chemical reaction products, which subsequently affect the interface interactions. In metals, the kinetics of oxidation can tip the balance between mild wear and severe wear. The effects of oxidation and reaction products can be even more significant to the tribological behavior of polymers; small and chemically modified debris fragments can adhere strongly to abrasive countersurfaces to create a stable, low-friction, and low-wear interface. Although the pathways and fundamental mechanisms leading to low friction and high wear resistance can vary widely for different materials, the formation of favorable surface films—tribofilms—is a critical aspect of tribological performance.

The past two decades have witnessed the development of increasingly sophisticated experimental tools intended to more directly probe molecular-scale processes. These tools have enabled systematic investigations of a wide range of environmental effects on single-asperity contacts composed of materials ranging from the practical and traditional to more exotic nanostructured and graded composites. The gaps between simulated and experimental length scales and timescales remain an important barrier to progress, although trends of experimental miniaturization and increasingly greater computing power are helping to bridge these gaps. The present cross section of recent advances demonstrates that, although tribology research has roots dating back five centuries, there is plenty of room at the interface for fundamental and impactful discovery.

DISCLOSURE STATEMENT

The authors are not aware of any affiliations, memberships, funding, or financial holdings that might be perceived as affecting the objectivity of this review.

LITERATURE CITED

1. Tomlinson GA. 1929. A molecular theory of friction. *Philos. Mag.* 7(46):905–39
2. Frenkel J, Kontorova T. 1939. On the theory of plastic deformation and twinning. *J. Phys. USSR* 1:137–49
3. Mate CM, McClelland GM, Erlandsson R, Chiang S. 1987. Atomic-scale friction of a tungsten tip on a graphite surface. *Phys. Rev. Lett.* 59(17):1942–45
4. Dienwiebel M, Pradeep N, Verhoeven GS, Zandbergen HW, Frenken JWM. 2005. Model experiments of superlubricity of graphite. *Surf. Sci.* 576(1–3):197–211
5. Dienwiebel M, Verhoeven GS, Pradeep N, Frenken JWM, Heimberg JA, Zandbergen HW. 2004. Superlubricity of graphite. *Phys. Rev. Lett.* 92(12):126101
6. Hirano M, Shinjo K, Kaneko R, Murata Y. 1997. Observation of superlubricity by scanning tunneling microscopy. *Phys. Rev. Lett.* 78(8):1448–51
7. Brukman MJ, Gao GT, Nemanich RJ, Harrison JA. 2008. Temperature dependence of single-asperity diamond-diamond friction elucidated using AFM and MD simulations. *J. Phys. Chem. C* 112(25):9358–69
8. He MY, Blum AS, Overney G, Overney RM. 2002. Effect of interfacial liquid structuring on the coherence length in nanolubrication. *Phys. Rev. Lett.* 88(15):154302
9. Schirmeisen A, Jansen L, Holscher H, Fuchs H. 2006. Temperature dependence of point contact friction on silicon. *Appl. Phys. Lett.* 88(12):123108
10. Zhao XY, Hamilton M, Sawyer WG, Perry SS. 2007. Thermally activated friction. *Tribol. Lett.* 27(1):113–17
11. Bennewitz R, Gyalog T, Guggisberg M, Bammerlin M, Meyer E, Guntherodt HJ. 1999. Atomic-scale stick-slip processes on Cu(111). *Phys. Rev. B* 60(16):R11301
12. Gnecco E, Bennewitz R, Gyalog T, Loppacher C, Bammerlin M, et al. 2000. Velocity dependence of atomic friction. *Phys. Rev. Lett.* 84(6):1172–75
13. Szlufarska I, Chandross M, Carpick RW. 2008. Recent advances in single-asperity nanotribology. *J. Phys. D* 41:123001
14. Sinnott SB, Heo S-J, Brenner DW, Harrison JA. 2007. Computer simulations of nanometer-scale indentation and friction. In *Springer Handbook on Nanotechnology*, ed. B Bhushan, pp. 1051–106. Heidelberg, Ger.: Springer-Verlag
15. Harrison JA, Stuart SJ, Brenner DW. 1999. Atomic-scale simulations of tribological and related phenomena. In *Handbook of Micro/Nanotribology*, ed. B Bhushan, pp. 525–94. Boca Raton, FL: CRC
16. Belak JF. 1993. Nanotribology. *MRS Bull.* 18(5):15–19
17. Belak J, Boercker DB, Stowers IF. 1993. Simulation of nanometer-scale deformation of metallic and ceramic surfaces. *MRS Bull.* 18(5):55–60

18. Landman U, Luedtke WD, Burnham NA, Colton RJ. 1990. Atomistic mechanisms and dynamics of adhesion, nanoindentation, and fracture. *Science* 248(4954):454–61
19. Landman U, Luedtke WD, Ringer EM. 1992. Atomistic mechanisms of adhesive contact formation and interfacial processes. *Wear* 153(1):3–30
20. Landman U, Luedtke WD, Gao JP. 1996. Atomic-scale issues in tribology: interfacial junctions and nano-elastohydrodynamics. *Langmuir* 12(19):4514–28
21. Komvopoulos K, Yan W. 1997. Molecular dynamics simulation of single and repeated indentation. *J. Appl. Phys.* 82(10):4823–30
22. Kelchner CL, Plimpton SJ, Hamilton JC. 1998. Dislocation nucleation and defect structure during surface indentation. *Phys. Rev. B* 58(17):11085–88
23. Isono Y, Tanaka T. 1997. Three-dimensional molecular dynamics simulation of atomic scale precision processing using a pin tool. *JSME Int. J. A* 40(3):211–18
24. Zhang L, Tanaka H. 1997. Towards a deeper understanding of wear and friction on the atomic scale—a molecular dynamics analysis. *Wear* 211:44–53
25. Fang T-H, Weng C-I. 2000. Three-dimensional molecular dynamics analysis of processing using a pin tool on the atomic scale. *Nanotechnology* 11:148–53
26. Lin Z-C, Huang J-C. 2004. A nano-orthogonal cutting model based on a modified molecular dynamics technique. *Nanotechnology* 15:510–19
27. Ye YY, Biswas R, Morris JR, Bastawros A, Chandra A. 2003. Molecular dynamics simulation of nanoscale machining of copper. *Nanotechnology* 14:390–96
28. Komanduri R, Chandrasekaran N, Raff LM. 2000. MD simulation of indentation and scratching of single crystal aluminum. *Wear* 240(1–2):113–43
29. Buldum A, Ciraci S. 1997. Atomic-scale study of dry sliding friction. *Phys. Rev. B* 55(4):2606–11
30. Isono Y, Tanaka T. 1999. Molecular dynamics simulations of atomic scale indentation and cutting process with atomic force microscopy. *JSME Int. J. A* 42(2):158–66
31. Yan Y, Sun T, Dong S, Liang Y. 2007. Study on effects of the feed on AFM-based nano-scratching process using MD simulation. *Comput. Mater. Sci.* 40:1–5
32. Gao GT, Mikulski PT, Harrison JA. 2002. Molecular-scale tribology of amorphous carbon coatings: effects of film thickness, adhesion, and long-range interactions. *J. Am. Chem. Soc.* 124(24):7202–9
33. Thompson PA, Robbins MO. 1990. Origin of stick-slip motion in boundary lubrication. *Science* 250(4982):792–94
34. Baljon ARC, Robbins MO. 1997. Adhesion and friction of thin films. *MRS Bull.* 22(1):22–26
35. Cieplak M, Smith ED, Robbins MO. 1994. Molecular origins of friction: the force on adsorbed layers. *Science* 265(5176):1209–12
36. Thompson PA, Grest GS, Robbins MO. 1992. Phase transitions and universal dynamics in confined films. *Phys. Rev. Lett.* 68(23):3448–51
37. Bhushan B, Israelachvili JN, Landman U. 1995. Nanotribology: friction, wear and lubrication at the atomic scale. *Nature* 374(6523):607–16
38. Jang I, Burris DL, Dickrell PL, Barry PR, Santos C, et al. 2007. Sliding orientation effects on the tribological properties of polytetrafluoroethylene. *J. Appl. Phys.* 102:123509
39. Erdemir A. 2005. Review of engineered tribological interfaces for improved boundary lubrication. *Tribol. Int.* 38(3):249–56
40. Erdemir A, Donnet C. 2006. Tribology of diamond-like carbon films: recent progress and future prospects. *J. Phys. D* 39(18):R311
41. Yang S, Camino D, Jones AHS, Teer DG. 2000. Deposition and tribological behaviour of sputtered carbon hard coatings. *Surf. Coat. Technol.* 124(2–3):110–16
42. Andersson L-P. 1981. A review of recent work on hard i-C films. *Thin Solid Films* 86(2–3):193–200
43. Holm R. 1929. Über metallische Kontaktwiderstände. *Wiss. Veroff. Siemens Werken* 7(2):217–58
44. Cocks M. 1962. Interaction of sliding metal surfaces. *J. Appl. Phys.* 33(7):2152–61
45. Greenwood JA. 1966. Constriction resistance and the real area of contact. *Br. J. Appl. Phys.* 17(12):1621
46. Tabor D. 1951. *The Hardness of Metals*. Oxford, UK: Clarendon
47. Antler M. 1980. Sliding wear of metallic contacts. *Proc. IEEE Holm Conf. Electr. Contacts, 26th*, pp. 3–24. Piscataway, NJ: IEEE

48. Antler M. 1964. Processes of metal transfer and wear. *Wear* 7(2):181–203
49. Blau PJ. 1997. Fifty years of research on the wear of metals. *Tribol. Int.* 30(5):321–31
50. Dickrell DJ. 2006. *Experimental investigation and numerical simulation of composite electrical contact materials for microelectromechanical systems applications*. PhD Thesis, Dep. Aerosp. Mech. Eng., Univ. Fla., Gainesville
51. Dickrell DJ, Dugger MT. 2007. Electrical contact resistance degradation of a hot-switched simulated metal MEMS contact. *Compon. Packag. Technol. IEEE Trans.* 30(1):75–80
52. Romig AD Jr, Dugger MT, McWhorter PJ. 2003. Materials issues in microelectromechanical devices: science, engineering, manufacturability and reliability. *Acta Mater.* 51(19):5837–66
53. Vincent ML, Chiesi JC, Fourrier A, Garnier B, Grappe C, et al. 2008. Electrical contact reliability in a magnetic MEMS switch. *Proc. IEEE Holm Conf. Electr. Contacts, 54th*, pp. 145–50. Piscataway, NJ: IEEE
54. Argibay N, Sawyer WG. 2012. Low wear metal sliding electrical contacts at high current density. *Wear* 274–75(0):229–37
55. Argibay N, Bares JA, Keith JH, Bourne GR, Sawyer WG. 2010. Copper-beryllium metal fiber brushes in high current density sliding electrical contacts. *Wear* 268(11–12):1230–36
56. Argibay N, Bares JA, Sawyer WG. 2009. Asymmetric wear behavior of self-mated copper fiber brush and slip-ring sliding electrical contacts in a humid carbon dioxide environment. *Wear* 268:455–63
57. Rigney DA. 2000. Transfer, mixing and associated chemical and mechanical processes during the sliding of ductile materials. *Wear* 245(1–2):1–9
58. Kuhlmann-Wilsdorf D. 1999. Metal fiber brushes. In *Electrical Contacts: Principles and Applications*, ed. PG Slade, pp. 943–1017. New York: Marcel Dekker
59. Rigney DA. 1997. Comments on the sliding wear of metals. *Tribol. Int.* 30(5):361–67
60. Boyer L, Noel S, Chabrerie JP. 1987. Electrochemically activated wear of metal fibre brushes. *Wear* 116:43–57
61. Johnson JL, Schreurs J. 1982. High-current brushes. Part VIII. Effect of electrical load. *Wear* 78:219–32
62. Boyer L, Chabrerie JP, Saint-Michel J. 1982. Low wear metallic fibre brushes. *Wear* 78(1–2):59–68
63. Haney PB, Kuhlmann-Wilsdorf D, Wilsdorf HGF. 1981. Production and performance of metal foil brushes. *Wear* 73(2):261–82
64. Reichner P. 1980. Metallic brushes for extreme high-current applications. *IEEE Trans. Compon. Hybrids Manuf. Technol.* 3(1):21–25
65. Dillich S, Kuhlmann-Wilsdorf D. 1980. Effects of surface films on the performance of silver-graphite (75 wt% Ag, 25 wt% C) electric brushes. *IEEE Trans. Compon. Hybrids Manuf. Technol.* 3(1):37–41
66. Johnson JL, Moberly LE, 1978. High-current brushes. Part I. Effect of brush and ring materials. *IEEE Trans. Compon. Hybrids Manuf. Technol.* 1(1):36–40
67. Johnson J, McKinney J. 1971. Electrical-power brushes for dry inert-gas atmospheres. *IEEE Trans. Parts Mater. Packag.* 7(1):62–69
68. Lim SC. 1998. Recent developments in wear-mechanism maps. *Tribol. Int.* 31(1–3):87–97
69. Lim SC, Ashby MF. 1987. Wear-mechanism maps. *Acta Metall.* 35:1–24
70. Shan Z, Stach EA, Wiezorek JMK, Knapp JA, Follstaedt DM, Mao SX. 2004. Grain boundary-mediated plasticity in nanocrystalline nickel. *Science* 305(5684):654–57
71. Schuh CA, Nieh TG, Yamasaki T. 2002. Hall–Petch breakdown manifested in abrasive wear resistance of nanocrystalline nickel. *Scr. Mater.* 46(10):735–40
72. Schiotz J, Di Tolla FD, Jacobsen KW. 1998. Softening of nanocrystalline metals at very small grain sizes. *Nature* 391(6667):561–63
73. Antler M. 1998. Gold-plated contacts: effect of thermal aging on contact resistance. *Plat. Surf. Finish.* 85(12):85–90
74. Argibay N, Brumbach MT, Dugger MT, Kotula PG. 2013. Grain boundary diffusivity of Ni in Au thin films and the associated degradation in electrical contact resistance due to surface oxide film formation. *J. Appl. Phys.* 113(11):114906–8
75. Pinnel M, Bennett J. 1972. Mass diffusion in polycrystalline copper/electroplated gold planar couples. *Metall. Mater. Trans. B* 3:1989–97
76. Reichner P. 1981. High current tests of metal fiber brushes. *IEEE Trans. Compon. Hybrids Manuf. Technol.* 4(1):2–4

77. Boyer L. 1984. Behaviour of fibre brushes under transient atmospheric conditions. *Wear* 93(3):299–317
78. Cabrera N, Mott NF. 1947. Theory of the oxidation of metals. *Rep. Prog. Phys.* 12:163–84
79. Fehlner FP, Mott NF. 1970. Low-temperature oxidation. *Oxid. Met.* 2:59–99
80. Bares JA, Argibay N, Mauntler N, Dudder GJ, Perry SS, et al. 2009. High current density copper-on-copper sliding electrical contacts at low sliding velocities. *Wear* 267(1–4):417–24
81. Argibay N, Sawyer W. 2012. Frictional voltammetry with copper. *Tribol. Lett.* 46(3):337–42
82. Jahanmir S, Suh NP. 1977. Mechanics of subsurface void nucleation in delamination wear. *Wear* 44(1):17–38
83. Suh NP. 1973. The delamination theory of wear. *Wear* 25(1):111–24
84. Suh NP. 1977. An overview of the delamination theory of wear. *Wear* 44(1):1–16
85. Argibay N. 2011. *Low wear metal sliding electrical contacts*. PhD Thesis, Dep. Mech. Aerosp. Eng., Univ. Fla., Gainesville
86. Roscoe R. 1926. The plastic deformation of cadmium single crystals. *Philos. Mag.* 21:399–406
87. Buckley DH. 1981. *Surface Effects in Adhesion, Friction, Wear, and Lubrication* (*Tribology Series 5*). Amsterdam: Elsevier Sci.
88. Shen H, Podlaseck SE, Kramer IR. 1966. Effect of vacuum on the fatigue life of aluminum. *Acta Metall.* 14(3):341–46
89. Wood WA, Cousland SM, Sargant KR. 1963. Systematic microstructural changes peculiar to fatigue deformation. *Acta Metall.* 11(7):643–52
90. Duquette D, Gell M. 1971. The effect of environment on the mechanism of Stage I fatigue fracture. *Metall. Mater. Trans. B* 2(5):1325–31
91. Nicola L, Xiang Y, Vlassak JJ, Van der Giessen E, Needleman A. 2006. Plastic deformation of free-standing thin films: experiments and modeling. *J. Mech. Phys. Solids* 54(10):2089–110
92. Mischler S. 2008. Triboelectrochemical techniques and interpretation methods in tribocorrosion: a comparative evaluation. *Tribol. Int.* 41(7):573–83
93. Pourbaix M. 1974. *Atlas of Electrochemical Equilibria in Aqueous Solutions*. Houston: Natl. Assoc. Corros. Eng. 2nd ed.
94. Celis JP, Ponthiaux P, Wenger F. 2006. Tribo-corrosion of materials: interplay between chemical, electrochemical, and mechanical reactivity of surfaces. *Wear* 261(9):939–46
95. Lo CC, Augis JA, Pinnel MR. 1979. Hardening mechanisms of hard gold. *J. Appl. Phys.* 50(11):6887–91
96. Yanson AI, Bollinger GR, Van den Brom HE, Agrait N, Van Ruitenbeek JM. 1998. Formation and manipulation of a metallic wire of single gold atoms. *Nature* 395(6704):783–85
97. Gosvami NN, Feldmann M, Peguiron Jl, Moseler M, Schirmeisen A, Bennewitz R. Ageing of a microscopic sliding gold contact at low temperatures. *Phys. Rev. Lett.* 107(14):144303
98. Yamakov V, Wolf D, Phillpot SR, Gleiter H. 2003. Dislocation-dislocation and dislocation-twin reactions in nanocrystalline Al by molecular dynamics simulation. *Acta Mater.* 51(14):4135–47
99. Yamakov V, Moldovan D, Rastogi K, Wolf D. 2006. Relation between grain growth and grain-boundary diffusion in a pure material by molecular dynamics simulations. *Acta Mater.* 54(15):4053–61
100. Wolf D, Yamakov V, Phillpot SR, Mukherjee A, Gleiter H. 2005. Deformation of nanocrystalline materials by molecular-dynamics simulation: relationship to experiments? *Acta Mater.* 53(1):1–40
101. Haslam AJ, Moldovan D, Yamakov V, Wolf D, Phillpot SR, Gleiter H. 2003. Stress-enhanced grain growth in a nanocrystalline material by molecular-dynamics simulation. *Acta Mater.* 51(7):2097–112
102. Haslam AJ, Phillpot SR, Wolf D, Moldovan D, Gleiter H. 2001. Mechanisms of grain growth in nanocrystalline fcc metals by molecular-dynamics simulation. *Mater. Sci. Eng. A* 318(1–2):293–312
103. Li Q, Dong Y, Perez D, Martini A, Carpick RW. 2011. Speed dependence of atomic stick-slip friction in optimally matched experiments and molecular dynamics simulations. *Phys. Rev. Lett.* 106(12):126101
104. Lo CC, Augis JA, Pinnel MR. 1979. Hardening mechanisms of hard gold. *J. Appl. Phys.* 50(11):6887–91
105. Argibay N, Prasad SV, Goeke RS, Dugger MT, Michael JR. 2013. Wear resistant electrically conductive Au–ZnO nanocomposite coatings synthesized by e-beam evaporation. *Wear* 302(1–2):955–62
106. Munitz A, Komem Y. 1980. The increase in the electrical resistance of heat-treated Au/Cr films. *Thin Solid Films* 71(2):177–88
107. Tompkins HG, Pinnel MR. 1977. Relative rates of nickel diffusion and copper diffusion through gold. *J. Appl. Phys.* 48(7):3144–46

108. Tompkins HG, Pinnel MR. 1976. Low temperature diffusion of copper through gold. *J. Appl. Phys.* 47(9):3804–12
109. Holloway PH, Amos DE, Nelson GC. 1976. Analysis of grain boundary diffusion in thin films: chromium in gold. *J. Appl. Phys.* 47(9):3769–75
110. Antler M. 1973. Tribological properties of gold for electric contacts. *IEEE Trans. Parts Hybrids Packag.* 9(1):4–14
111. Okinaka Y, Hoshino M. 1998. Some recent topics in gold plating for electronics applications. *Gold Bull.* 31(1):3–13
112. Rigney DA, Hirth JP. 1979. Plastic deformation and sliding friction of metals. *Wear* 53(2):345–70
113. Padilla HA II, Boyce BL, Battaile CC, Prasad SV. 2013. Frictional performance and near-surface evolution of nanocrystalline Ni-Fe as governed by contact stress and sliding velocity. *Wear* 297(1–2):860–71
114. Prasad SV, Battaile CC, Kotula PG. 2010. Friction transitions in nanocrystalline nickel. *Scr. Mater.* 64(8):729–32
115. Prasad SV, Michael JR, Christenson TR. 2003. EBSD studies on wear-induced subsurface regions in LIGA nickel. *Scr. Mater.* 48(3):255–60
116. Padilla HA II, Boyce BL. 2010. A review of fatigue behavior in nanocrystalline metals. *Exp. Mech.* 50(1):5–23
117. Asay D, Dugger M, Kim S. 2008. In-situ vapor-phase lubrication of MEMS. *Tribol. Lett.* 29(1):67–74
118. Argibay N, Keith J, Krick B, Hahn D, Bourne G, Sawyer W. 2010. High-temperature vapor phase lubrication using carbonaceous gases. *Tribol. Lett.* 40(1):3–9
119. Chookajorn T, Murdoch HA, Schuh CA. 2012. Design of stable nanocrystalline alloys. *Science* 337(6097):951–54
120. Dunn AC, Steffens JG, Burris DL, Banks SA, Sawyer WG. 2008. Spatial geometric effects on the friction coefficients of UHMWPe. *Wear* 264(7):648–53
121. Wang A, Stark C, Dumbleton JH. 1996. Mechanistic and morphological origins of ultra-high molecular weight polyethylene wear debris in total joint replacement prostheses. *Proc. Inst. Mech. Eng. H* 210(3):141–55
122. Hamilton MA, Banks SA, Sawyer WG, Sucec MC, Fregly BJ. 2005. Quantifying multidirectional sliding motions in total knee replacements. *J. Tribol.* 127(2):280–86
123. Burris DL, Boesl B, Bourne GR, Sawyer WG. 2007. Polymeric nanocomposites for tribological applications. *Macromol. Mater. Eng.* 292(4):387–402
124. Lancaster JK. 1972. Polymer-based bearing materials: role of fillers and fiber reinforcement in wear. *Wear* 22(3):249–55
125. Sung N, Suh N. 1979. Effect of fiber orientation on friction and wear of fiber reinforced polymeric composites. *Wear* 53(1):129–41
126. Schmitz T, Action J, Burris D, Ziegert J, Sawyer W. 2004. Wear-rate uncertainty analysis. *J. Tribol. Trans. ASME* 126(4):802–8
127. Burris D, Sawyer W. 2006. A low friction and ultra low wear rate PEEK/PTFE composite. *Wear* 261(3–4):410–18
128. Tanaka K, Uchiyama Y, Toyooka S. 1973. Mechanism of wear of polytetrafluoroethylene. *Wear* 23(2):153–72
129. Bahadur S, Tabor D. 1984. The wear of filled polytetrafluoroethylene. *Wear* 98(1–3):1–13
130. Blanchet T, Kennedy F. 1992. Sliding wear mechanism of polytetrafluoroethylene (PTFE) and PTFE composites. *Wear* 153(1):229–43
131. Tanaka K, Kawakami S. 1982. Effect of various fillers on the friction and wear of polytetrafluoroethylene-based composites. *Wear* 79(2):221–34
132. Wang O, Xue Q, Shen W. 1997. The friction and wear properties of nanometre SiO_2 filled polyetheretherketone. *Tribol. Int.* 30(3):193–97
133. Wang Q, Xu J, Shen W, Liu W. 1996. An investigation of the friction and wear properties of nanometer Si_3N_4 filled PEEK. *Wear* 196(1–2):82–86
134. Wang Q, Xue Q, Liu H, Shen W, Xu J. 1996. The effect of particle size of nanometer ZrO_2 on the tribological behaviour of PEEK. *Wear* 198(1–2):216–19

135. Wang Q, Xue Q, Liu W, Chen J. 2000. The friction and wear characteristics of nanometer SiC and polytetrafluoroethylene filled polyetheretherketone. *Wear* 243(1–2):140–46
136. Xue Q, Wang Q. 1997. Wear mechanisms of polyetheretherketone composites filled with various kinds of SiC. *Wear* 213(1–2):54–58
137. Li F, Hu K, Li J, Zhao B. 2001. The friction and wear characteristics of nanometer ZnO filled polytetrafluoroethylene. *Wear* 249(10–11):877–82
138. Chen W, Li F, Han G, Xia J, Wang L, et al. 2003. Tribological behavior of carbon-nanotube-filled PTFE composites. *Tribol. Lett.* 15(3):275–78
139. Sawyer W, Freudenberg K, Bhimaraj P, Schadler L. 2003. A study on the friction and wear behavior of PTFE filled with alumina nanoparticles. *Wear* 254(5–6):573–80
140. Burris D, Sawyer W. 2005. Tribological sensitivity of PTFE/alumina nanocomposites to a range of traditional surface finishes. *Tribol. Trans.* 48(2):147–53
141. Burris DL, Zhao S, Duncan R, Lowitz J, Perry SS, et al. 2009. A route to wear resistant PTFE via trace loadings of functionalized nanofillers. *Wear* 267(1–4):653–60
142. McElwain S. 2006. *Wear resistant PTFE composites via nano-scale particles*. Master's Thesis, Rensselaer Polytech. Inst., Troy, NY
143. McElwain S, Blanchet T, Schadler L, Sawyer W. 2008. Effect of particle size on the wear resistance of alumina-filled PTFE micro- and nanocomposites. *Tribol. Trans.* 51(3):247–53
144. Blanchet TA, Kandanur SS, Schadler LS. 2010. Coupled effect of filler content and countersurface roughness on PTFE nanocomposite wear resistance. *Tribol. Lett.* 40(1):11–21
145. Krick BA, Ewin JJ, Blackman GS, Junk CP, Sawyer WG. 2012. Environmental dependence of ultra-low wear behavior of polytetrafluoroethylene (PTFE) and alumina composites suggests tribochemical mechanisms. *Tribol. Int.* 51:42–46
146. Burris D, Sawyer W. 2006. Improved wear resistance in alumina-PTFE nanocomposites with irregular shaped nanoparticles. *Wear* 260(7–8):915–18
147. Bahadur S, Gong D. 1992. The action of fillers in the modification of the tribological behavior of polymers. *Wear* 158(1–2):41–59
148. Burroughs B, Kim J, Blanchet T. 1999. Boric acid self-lubrication of B_2O_3-filled polymer composites. *Tribol. Trans.* 42(3):592–600
149. Li F, Yan F, Yu L, Liu W. 2000. The tribological behaviors of copper-coated graphite filled PTFE composites. *Wear* 237(1):33–38
150. Lu Z, Friedrich K. 1995. On sliding friction and wear of PEEK and its composites. *Wear* 181:624–31
151. Menzel B, Blanchet T. 2002. Effect of particle size and volume fraction of irradiated FEP filler on the transfer wear of PTFE. *Lubr. Eng.* 58(9):29–35
152. Agag T, Koga T, Takeichi T. 2001. Studies on thermal and mechanical properties of polyimide-clay nanocomposites. *Polymer* 42(8):3399–408
153. Eitan A, Fisher F, Andrews R, Brinson L, Schadler L. 2006. Reinforcement mechanisms in MWCNT-filled polycarbonate. *Compos. Sci. Technol.* 66(9):1162–73
154. He P, Gao Y, Lian J, Wang L, Qian D, et al. 2006. Surface modification and ultrasonication effect on the mechanical properties of carbon nanofiber/polycarbonate composites. *Composites A* 37(9):1270–75
155. Fornes TD, Yoon PJ, Keskkula H, Paul DR. 2001. Nylon 6 nanocomposites: the effect of matrix molecular weight. *Polymer* 42(25):9929–40
156. Gacitua WE, Ballerini AA, Zhang J. 2005. Polymer nanocomposites: synthetic and natural fillers: a review. *Maderas Cienc. Tecnol.* 7(3):159–78
157. Hussain F, Hojjati M, Okamoto M, Gorga RE. 2006. Review article: polymer-matrix nanocomposites, processing, manufacturing, and application: an overview. *J. Compos. Mater.* 40(17):1511–75
158. Kuchta F-D, Lemstra PJ, Kellar A, Batenburg LF, Fisher HR. 1999. Materials with improved properties from polymer-ceramic nanocomposites. *MRS Proc.* 576:363–68
159. Petrovicova E, Knight R, Schadler L, Twardowski T. 2000. Nylon 11/silica nanocomposite coatings applied by the HVOF process. II. Mechanical and barrier properties. *J. Appl. Polym. Sci.* 78(13):2272–89
160. Reynaud E, Jouen T, Gauthier C, Vigier G, Varlet J. 2001. Nanofillers in polymeric matrix: a study on silica reinforced PA6. *Polymer* 42(21):8759–68

161. Thostenson ET, Li CY, Chou TW. 2005. Nanocomposites in context. *Compos. Sci. Technol.* 65(3–4):491–516
162. Thostenson ET, Ren ZF, Chou TW. 2001. Advances in the science and technology of carbon nanotubes and their composites: a review. *Compos. Sci. Technol.* 61(13):1899–912
163. Yasmin A, Luo J, Abot J, Daniel I. 2006. Mechanical and thermal behavior of clay/epoxy nanocomposites. *Compos. Sci. Technol.* 66:2415–22
164. Zhu A, Sternstein S. 2003. Nonlinear viscoelasticity of nanofilled polymers: interfaces, chain statistics and properties recovery kinetics. *Compos. Sci. Technol.* 63(8):1113–26
165. Kojima Y, Usuki A, Kawasumi M, Okada A, Fukushima Y, et al. 1993. Mechanical-properties of nylon 6–clay hybrid. *J. Mater. Res.* 8(5):1185–89
166. Yang H, Bhimaraj P, Siegel R, Schadler L. 2007. Crystal growth in alumina/poly(ethylene terephthalate) nanocomposite films. *J. Polym. Sci. B* 45(7):747–57
167. Xiao Z, Li Y, Ma D, Schadler L, Akpalu Y. 2006. Probing the use of small-angle light scattering for characterizing structure of titanium dioxide/low-density polyethylene nanocomposites. *J. Polym. Sci. B* 44(7):1084–95
168. Petrovicova E, Knight R, Schadler L, Twardowski T. 2000. Nylon 11/silica nanocomposite coatings applied by the HVOF process. I. Microstructure and morphology. *J. Appl. Polym. Sci.* 77(8):1684–99
169. Ash B, Schadler L, Siegel R. 2002. Glass transition behavior of alumina/polymethylmethacrylate nanocomposites. *Mater. Lett.* 55(1–2):83–87
170. Maiti M, Bhowmick A. 2006. New insights into rubber-clay nanocomposites by AFM imaging. *Polymer* 47(17):6156–66
171. Brown E, Rae P, Orler E, Gray G, Dattelbaum D. 2006. The effect of crystallinity on the fracture of polytetrafluoroethylene (PTFE). *Mater. Sci. Eng. C* 26(8):1338–43
172. Joyce J. 2003. Fracture toughness evaluation of polytetrafluoroethylene. *Polym. Eng. Sci.* 43(10):1702–14
173. Brown E, Dattelbaum D. 2005. The role of crystalline phase on fracture and microstructure evolution of polytetrafluoroethylene (PTFE). *Polymer* 46(9):3056–68
174. Rae P, Brown E. 2005. The properties of poly(tetrafluoroethylene) (PTFE) in tension. *Polymer* 46(19):8128–40
175. Rae P, Dattelbaum D. 2004. The properties of poly(tetrafluoroethylene) (PTFE) in compression. *Polymer* 45(22):7615–25
176. Makinson KR, Tabor D. 1964. Friction + transfer of polytetrafluoroethylene. *Nature* 201(491):464–66
177. Clark E. 1999. The molecular conformations of polytetrafluoroethylene: forms II and IV. *Polymer* 40(16):4659–65
178. Weeks J, Clark E, Eby R. 1981. Crystal-structure of the low-temperature phase (II) of polytetrafluoroethylene. *Polymer* 22(11):1480–86
179. Tieyuan F, Zhishen M, Han P, Yuchen Q. 1986. Study of factors affecting room temperature transition of polytetrafluoroethylene. *Chin. J. Polym. Sci.* 2:170–79
180. Kimmig M, Strobl G, Stuhn B. 1994. Chain reorientation in poly(tetrafluoroethylene) by mobile twin-helix reversal defects. *Macromolecules* 27(9):2481–95
181. Marega C, Marigo A, Causin V, Kapeliouchko V, Di Nicolo E, Sanguineti A. 2004. Relationship between the size of the latex beads and the solid-solid phase transitions in emulsion polymerized poly(tetrafluoroethylene). *Macromolecules* 37(15):5630–37
182. D'Amore M, Auriemma F, De Rosa C, Barone V. 2004. Disordered chain conformations of poly(tetrafluoroethylene) in the high-temperature crystalline form I. *Macromolecules* 37(25):9473–80
183. Burris DL, Santos K, Lewis SL, Liu X, Perry SS, et al. 2008. Polytetrafluoroethylene matrix nanocomposites for tribological applications. In *Tribology of Polymeric Nanocomposites*, Vol. 55, ed. K Friedrich, AK Schlarb, pp. 403–38. Amsterdam: Elsevier
184. Basu SK, Tewari A, Fasulo PD, Rodgers WR. 2007. Transmission electron microscopy based direct mathematical quantifiers for dispersion in nanocomposites. *Appl. Phys. Lett.* 91:053105
185. Fagan JA, Landi BJ, Mandelbaum I, Simpson JR, Bajpai V, et al. 2006. Comparative measures of single-wall carbon nanotube dispersion. *J. Phys. Chem. B* 110(47):23801–5
186. Kashiwagi T, Fagan J, Douglas JF, Yamamoto K, Heckert AN, et al. 2007. Relationship between dispersion metric and properties of PMMA/SWNT nanocomposites. *Polymer* 48(16):4855–66

187. Li ZF, Luo GH, Zhou WP, Wei F, Xiang R, Liu YP. 2006. The quantitative characterization of the concentration and dispersion of multi-walled carbon nanotubes in suspension by spectrophotometry. *Nanotechnology* 17(15):3692–98
188. Lillehei PT, Kim JW, Gibbons LJ, Park C. 2009. A quantitative assessment of carbon nanotube dispersion in polymer matrices. *Nanotechnology* 20(32):325708
189. Luo ZP, Koo JH. 2007. Quantifying the dispersion of mixture microstructures. *J. Microsc.* 225(2):118–25
190. Luo ZP, Koo JH. 2008. Quantification of the layer dispersion degree in polymer layered silicate nanocomposites by transmission electron microscopy. *Polymer* 49(7):1841–52
191. Luo ZP, Koo JH. 2008. Quantitative study of the dispersion degree in carbon nanofiber/polymer and carbon nanotube/polymer nanocomposites. *Mater. Lett.* 62(20):3493–96
192. Navarchian AH, Majdzadeh-Ardakani K. 2009. Processing of transmission electron microscope images for quantification of the layer dispersion degree in polymer-clay nanocomposites. *J. Appl. Polym. Sci.* 114(1):531–42
193. Pegel S, Potschke P, Villmow T, Stoyan D, Heinrich G. 2009. Spatial statistics of carbon nanotube polymer composites. *Polymer* 50(9):2123–32
194. Tscheschel A, Lacayo J, Stoyan D. 2005. Statistical characterization of TEM images of silica-filled rubber. *J. Microsc.* 217:75–82
195. Khare HS, Burris DL. 2010. A quantitative method for measuring nanocomposite dispersion. *Polymer* 51(3):719–29
196. Ye J, Khare HS, Burris DL. 2013. Transfer film evolution and its role in promoting ultra-low wear of a PTFE nanocomposite. *Wear* 297(1–2):1095–102
197. Pitenis AA, Krick BA, Ewin JJ, Harris KL, Sawyer WG. 2014. In vacuo tribological behavior of polytetrafluoroethylene (PTFE) and alumina nanocomposites: the importance of water for ultra-low wear. *Tribol. Lett.* 53(1):189–97
198. Krick BA, Hahn DW, Sawyer WG. 2013. Plasmonic diagnostics for tribology: in situ observations using surface plasmon resonance in combination with surface-enhanced Raman spectroscopy. *Tribol. Lett.* 49(1):95–102
199. Fischer TE. 1988. Tribochemistry. *Annu. Rev. Mater. Sci.* 18:303–23
200. Biswas SK, Vijayan K. 1992. Friction and wear of PTFE—a review. *Wear* 158(1–2):193–211
201. Brainard WA, Buckley DH. 1973. Adhesion and friction of PTFE in contact with metals as studied by Auger spectroscopy, field ion and scanning electron microscopy. *Wear* 26(1):75–93
202. Cadman P, Gossedge GM. 1979. The chemical nature of metal-polytetrafluoroethylene tribological interactions as studied by X-ray photoelectron spectroscopy. *Wear* 54(2):211–15
203. Deli G, Qunji X, Hongli W. 1991. ESCA study on tribochemical characteristics of filled PTFE. *Wear* 148(1):161–69
204. Gong DL, Zhang B, Xue QJ, Wang HL. 1990. Effect of tribochemical reaction of polytetrafluoroethylene transferred film with substrates on its wear behavior. *Wear* 137(2):267–73
205. Jintang G, Hongxin D. 1988. Molecule structure variations in friction of stainless steel/PTFE and its composite. *J. Appl. Polym. Sci.* 36(1):73–85
206. Kajdas CK. 2005. Importance of the triboemission process for tribochemical reaction. *Tribol. Int.* 38(3):337–53
207. Li F, Yan FY, Yu LG, Liu WM. 2000. The tribological behaviors of copper-coated graphite filled PTFE composites. *Wear* 237(1):33–38
208. Majzner M, Kajdas C. 2003. Reactions of carboxylic acids under boundary friction conditions. *Tribol. Tarcie Zużycie Smarowanie* 2003:63–80
209. Matsunuma S. 1997. The initial step of tribochemical reactions of perfluoropolyether on amorphous carbon. *Wear* 213(1):112–16
210. Onodera T, Park M, Souma K, Ozawa N, Kubo M. 2013. Transfer-film formation mechanism of polytetrafluoroethylene: a computational chemistry approach. *J. Phys. Chem. C* 117(20):10464–72
211. Krick BA, Ewin JJ, McCumiskey EJ. 2014. Tribofilm formation and run-in behavior in ultra-low wearing polytetrafluoroethylene (PTFE) and alumina nanocomposites. Submitted to *Tribol. Trans.*
212. Erdemir A. 1993. A review of the lubrication of ceramics with thin solid films. In *Friction and Wear of Ceramics*, ed. S Jahanmir, pp. 119–62. New York: Marcel Dekker

213. Kato K. 1990. Tribology of ceramics. *Wear* 136(1):117–33
214. Erdemir A. 2000. A crystal-chemical approach to lubrication by solid oxides. *Tribol. Lett.* 8(2–3):97–102
215. Erdemir A. 2005. A crystal chemical approach to the formulation of self-lubricating nanocomposite coatings. *Surf. Coat. Technol.* 200(5–6):1792–96
216. Bucholz E, Kong C, Marchman K, Sawyer WG, Phillpot S, et al. 2012. Data-driven model for estimation of friction coefficient via informatics methods. *Tribol. Lett.* 47(2):211–21
217. Sawyer WG, Wahl KJ. 2008. Accessing inaccessible interfaces: in situ approaches to materials tribology. *MRS Bull.* 33(12):1145–48
218. Bennewitz R. 2005. Friction force microscopy. *Mater. Today* 8(5):42–48
219. Gnecco E, Bennewitz R, Meyer E. 2002. Abrasive wear on the atomic scale. *Phys. Rev. Lett.* 88(21):215501
220. Maier S, Pfeiffer O, Glatzel T, Meyer E, Filleter T, Bennewitz R. 2007. Asymmetry in the reciprocal epitaxy of NaCl and KBr. *Phys. Rev. B* 75(19):195408
221. Bennewitz R, Gnecco E, Gyalog T, Meyer E. 2001. Atomic friction studies on well-defined surfaces. *Tribol. Lett.* 10(1–2):51–56
222. Maier S, Gnecco E, Baratoff A, Bennewitz R, Meyer E. 2008. Atomic-scale friction modulated by a buried interface: combined atomic and friction force microscopy experiments. *Phys. Rev. B* 78(4):045432
223. Gnecco E, Bennewitz R, Gyalog T, Meyer E. 2001. Friction experiments on the nanometre scale. *J. Phys. Condens. Matter* 13(31):R619
224. Zhao X, Perry S. 2010. Temperature-dependent atomic scale friction and wear on PbS(100). *Tribol. Lett.* 39(2):169–75
225. Gnecco E, Bennewitz R, Gyalog T, Loppacher C, Bammerlin M, et al. 2000. Velocity dependence of atomic friction. *Phys. Rev. Lett.* 84(6):1172–75
226. Gnecco E, Bennewitz R, Socoliuc A, Meyer E. 2003. Friction and wear on the atomic scale. *Wear* 254(9):859–62
227. Howald L, Lüthi R, Meyer E, Gerth G, Haefke H, et al. 1994. Friction force microscopy on clean surfaces of NaCl, NaF, and AgBr. *J. Vac. Sci. Technol. B* 12(3):2227–30
228. Meyer E, Lüthi R, Howald L, Bammerlin M, Guggisberg M, Güntherodt HJ. 1996. Site-specific friction force spectroscopy. *J. Vac. Sci. Technol. B* 14(2):1285–88
229. Liley M, Gourdon D, Stamou D, Meseth U, Fischer TM, et al. 1998. Friction anisotropy and asymmetry of a compliant monolayer induced by a small molecular tilt. *Science* 280(5361):273–75
230. Hölscher H, Schwarz UD, Wiesendanger R. 1996. Simulation of a scanned tip on a NaF(001) surface in friction force microscopy. *Europhys. Lett.* 36(1):19
231. Fusco C, Fasolino A. 2005. Velocity dependence of atomic-scale friction: a comparative study of the one- and two-dimensional Tomlinson model. *Phys. Rev. B* 71(4):045413
232. Nakamura J, Wakunami S, Natori A. 2005. Double-slip mechanism in atomic-scale friction: Tomlinson model at finite temperatures. *Phys. Rev. B* 72(23):235415
233. Steiner P, Roth R, Gnecco E, Baratoff A, Meyer E. 2010. Angular dependence of static and kinetic friction on alkali halide surfaces. *Phys. Rev. B* 82(20):205417
234. Shluger AL, Williams RT, Rohl AL. 1995. Lateral and friction forces originating during force microscope scanning of ionic surfaces. *Surf. Sci.* 343(3):273–87
235. Yoshimichi N, Hitoshi S. 2000. Frictional force microscopic anisotropy on (001) surfaces of alkali halides and MgO. *Jpn. J. Appl. Phys.* 39(7S):4497
236. Livshits AI, Shluger AL. 1997. Self-lubrication in scanning-force-microscope image formation on ionic surfaces. *Phys. Rev. B* 56(19):12482–89
237. Trevethan T, Kantorovich L. 2004. Physical dissipation mechanisms in non-contact atomic force microscopy. *Nanotechnology* 15(2):S44
238. Steijn RP. 1964. Friction and wear of single crystals. *Wear* 7(1):48–66
239. Bowden FP, Brookes CA, Hanwell AE. 1964. Anisotropy of friction in crystals. *Nature* 203:27–30
240. Erdemir A. 2000. A crystal-chemical approach to lubrication by solid oxides. *Tribol. Lett.* 8(2):97–102